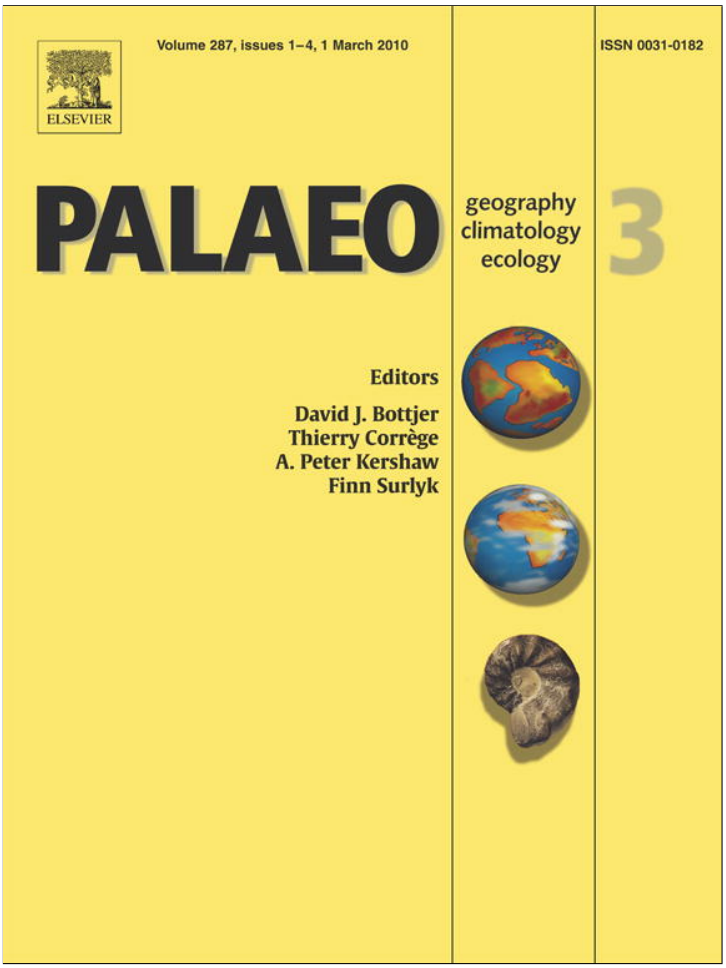

Palaeogeography, Palaeoclimatology, Palaeoecology 287 (2010) 1–27

Contents lists available at ScienceDirect

Palaeogeography, Palaeoclimatology, Palaeoecology

journal homepage: www.elsevier.com/locate/palaeo

Diatom distribution in southeastern Pacific surface sediments and their relationship to modern environmental variables

Oliver Esper *, Rainer Gersonde, Nicole Kadagies

Alfred-Wegener-Institute for Polar and Marine Research, Columbusstrasse, D-27568 Bremerhaven, Germany

ARTICLE INFO

Article history:
Received 24 June 2009
Received in revised form 23 November 2009
Accepted 6 December 2009
Available online 16 December 2009

Keywords:
Diatoms
Marine sediments
Amundsen Sea
Bellingshausen Sea
Antarctic Circumpolar Current
Canonical redundancy analysis

ABSTRACT

The quantitative analysis of diatom assemblages preserved in 52 samples from the Bellingshausen and the Amundsen Seas provides the first comprehensive view on the distribution of diatoms in surface sediments of the eastern and central Pacific sector of the Southern Ocean. On a latitudinal transect along 120°W, diatom valve accumulation rates (AR) reach maximum values ($8–10\times10^8$ valves m^{-2} yr^{-1}) in a zone extending over ca. 900 km between the Antarctic Polar Front and the maximum average winter sea ice extent and exceed those ARs obtained from an eastern transect along 90°W by one order of magnitude. Lowest diatom concentrations ($1–3\times10^6$ valves g^{-1}) were encountered in sediments of the Sea Ice Zone, affected by winter and summer sea ice. The accumulation rate pattern of the most abundant diatom *Fragilariopsis kerguelensis* (>50% abundance in 47 samples) mirrors the pattern of the total diatom valve AR and the biogenic silica (BSi) AR, making *F. kerguelensis* the major contributor to the BSi preserved at the sea floor. Relative abundances of diatom species and species groups were statistically compared with a selection of environmental variables, such as the mean summer sea surface temperature and salinity, mean annual surface nutrient concentration (nitrate, phosphate, silicon), mean annual water column stratification, mixed layer depth in summer, and mean summer and winter sea ice concentrations. Polynomial canonical redundancy analysis (RDA) revealed the biogeographic distribution of diatom species had the strongest relationship with summer sea surface temperature (SSST) out of the nine tested environmental variables. This relationship accounted for 69.6% of the total variance of the diatom distribution, with 29.7% explained by the first gradient (significantly correlated to SSST with $r^2=0.941$) and 15.6% explained by the second gradient (correlated to both summer and winter sea ice and silicon concentration). *Azpeitia tabularis, Hemidiscus cuneiformis* and *Roperia tesselata* were associated with warmer water conditions (>4 °C), whereas *Fragilariopsis curta*, *F. separanda*, *F. rhombica* and *Thalassiosira gracilis* were correlated with cold SSST (<1.5 °C). Under the second gradient relationship, *Actinocyclus actinochilus* and *F. curta* were the most important diatoms representative of the diatom distribution in relation to the observed mean summer and winter sea ice concentrations.
Confirming these environmental relationships is crucial for the development of reference data sets used in quantitative estimations of palaeoclimatic and palaeoceanographic conditions with statistical methods. This new data set represents the first modernised treatment of diatom remains from the SE Pacific Ocean and generally supports the use of a circum-polar database for the determination of summer SST, sea ice and potentially biogenic silica distribution of the Southern Ocean back into the Late Quaternary.

1. Introduction

The establishment of quantitative data sets on the diatom species composition preserved in Southern Ocean surface sediments (Zielinski and Gersonde, 1997; Pichon et al., 1998; Armand et al., 2005; Crosta et al., 2005; Romero et al., 2005) has allowed for the development of diatom-based transfer functions, which can be used to quantitatively reconstruct past Southern Ocean surface temperatures and sea ice concentrations (Pichon et al., 1987, 1992a,b, 1998; Zielinski et al., 1998; Crosta et al., 1998a,b) and for the definition of species abundance patterns as a template for the estimation of past sea ice distribution (Gersonde and Zielinski, 2000) and productivity regimes (Abelmann et al., 2006). Most of our understanding of Pleistocene Southern Ocean sea surface temperature (SST) and sea ice conditions at specific time slices and glacial/interglacial variability comes from diatom transfer function-based reconstructions (Crosta et al., 1998a,b, 2004; Zielinski et al., 1998; Bianchi and Gersonde, 2002, 2004; Kunz-Pirrung et al., 2002; Gersonde et al., 2003a,b, 2005; Armand and Leventer, 2003, 2009). Although this approach has essentially met with success, further studies are required to enhance our ability to reconstruct past Southern Ocean surface water conditions. This concerns primarily the extension of the diatom reference data sets into the Pacific sector, as requested by Gersonde et al. (2005), combined with a statistical

* Corresponding author. Tel.: +49 471 4831 1077; fax: +49 471 4831 1923.
E-mail address: Oliver.Esper@awi.de (O. Esper).

0031-0182/$ – see front matter © 2010 Elsevier B.V. All rights reserved.
doi:10.1016/j.palaeo.2009.12.006

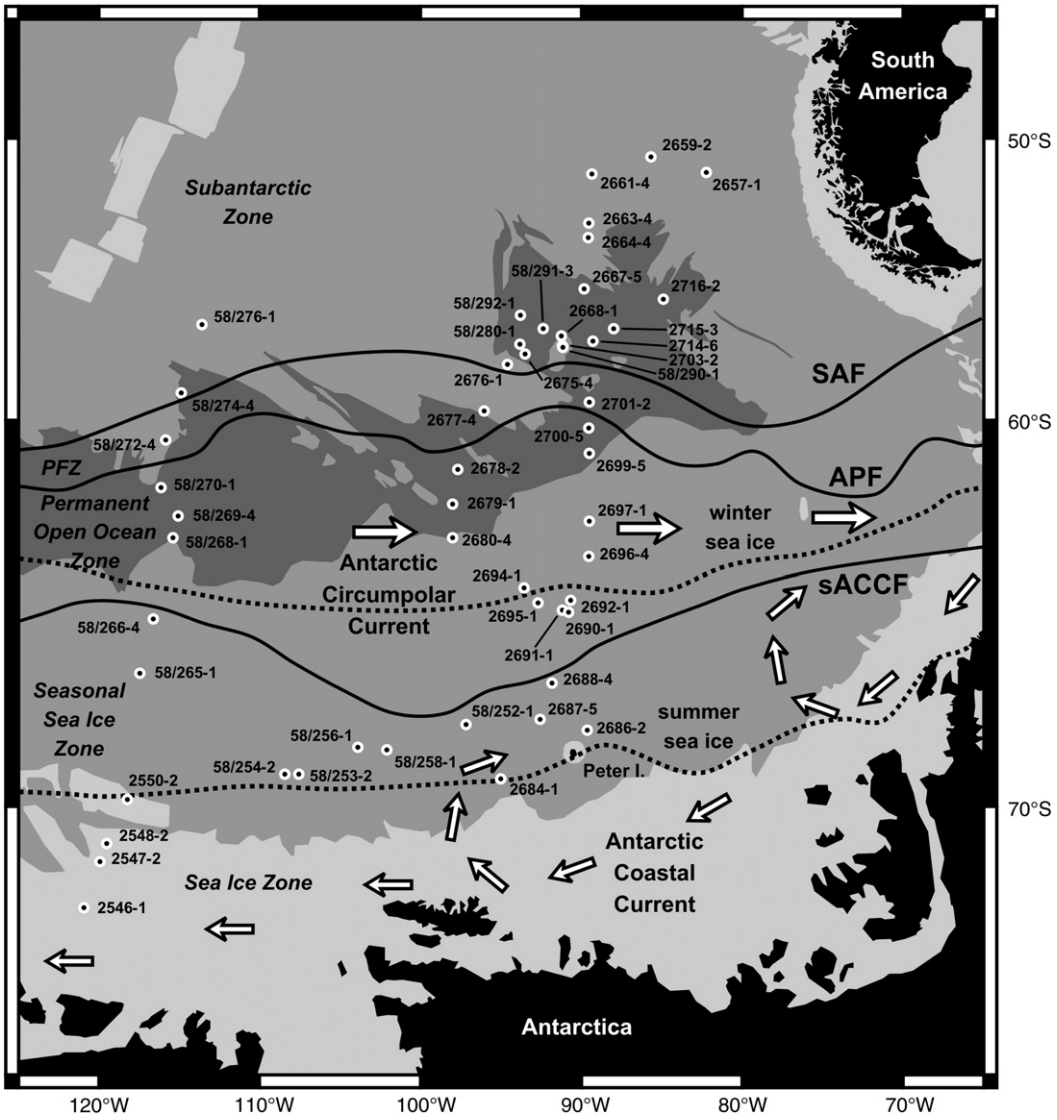

Fig. 1. Present-day surface oceanography in the Pacific sector of the Southern Ocean with the positions of the oceanic fronts (after Orsi et al., 1995; SAF: Subantarctic Front; APF: Antarctic Polar Front; PFZ: Polar Front Zone; sACCF: Southern ACC Front), the main sea surface currents (arrows; after Read et al., 1995; Nechaev et al., 1997; Smith et al., 1999), summer and winter sea ice extent (dashed lines; after Schweitzer, 1995), the bathymetry of the observed area (light grey: < 3000 m, medium grey: 3000–5000 m, dark grey: > 5000 m; taken from GEBCO: the General Bathymetric Chart of the Oceans) and the 52 sample positions.

verification of the relationship between environmental variables and the distribution of diatoms in modern sediments.

Although the Pacific sector of the Southern Ocean is the largest of the Southern Ocean sectors, modern studies of the distribution of diatoms preserved in the sedimentary record relevant to this Pacific sector have been restricted to coastal environments and basins along the Antarctic Peninsula (Crosta et al., 1997; Zielinski and Gersonde, 1997), the Amundsen Sea shelf (Kellogg and Kellogg, 1987) and the Ross Sea (Cunningham and Leventer, 1998) rather than venturing into the Antarctic Circumpolar Current (ACC). South Pacific open-ocean assemblages have been presented by Kozlova (1966) and Donahue (1973) and recently from a limited number of sites by Armand et al. (2005), Crosta et al. (2005) and Romero et al. (2005). In contrast, detailed studies of diatoms from South Pacific surface waters have been undertaken (e.g. Frenguelli and Orlando, 1958; Kozlova, 1966; Hargraves, 1968; Hasle, 1969; Fenner et al., 1976; Hasle, 1976; Burckle et al., 1987; Savidge et al., 1995; de Baar et al., 1999). In the absence of a reference data set for this area, palaeoenvironmental reconstructions based on diatom transfer functions rest on the assumption and earlier dispersal observations (e.g. Discovery reports by Hart, 1934; Hendey, 1937; Baker, 1954) that diatom distributions are circumpolar in character, that is, that the distribution of the Atlantic and Indian sectors can be extrapolated to the Pacific sector of the Southern Ocean. By confirming that the general zonal pattern of diatom distribution continues through the Pacific sector, palaeoceanographers could confidently support the pooling and application of reference data sets across the Southern Ocean for statistical analysis of core data from all sectors.

Here we present a comprehensive documentation of the diatom species distribution in the central and eastern Pacific sector of the Southern Ocean. We examined 52 surface sediment samples collected from two transects around 120°W and 90°W between the central ACC and the Antarctic near-shore coast (minimum water depths of about 2000 m) (Fig. 1). Considering that the sea-floor diatom assemblage compositions

Fig. 2. Environmental and physical variables characterising the (sub)surface water layer of the working area. Environmental variables are the mean sea surface summer temperature (TEMP; panel a) and the mean annual sea surface salinity (SAL; panel b), the mean annual dissolved nitrate concentration (NO_3; panel c), the mean annual dissolved phosphate concentration (PO_4; panel d) and the mean annual dissolved silicon concentration (Si; panel e). Physical variables include the summer mixed layer depth (MLD; panel f) and the mean annual stratification of the upper water column between 0 and 75 m expressed as Brunt–Väisälä-frequencies (N; panel g), the mean winter sea ice concentration (WSIC; panel h) and the mean summer sea ice concentration (SSIC; panel i).

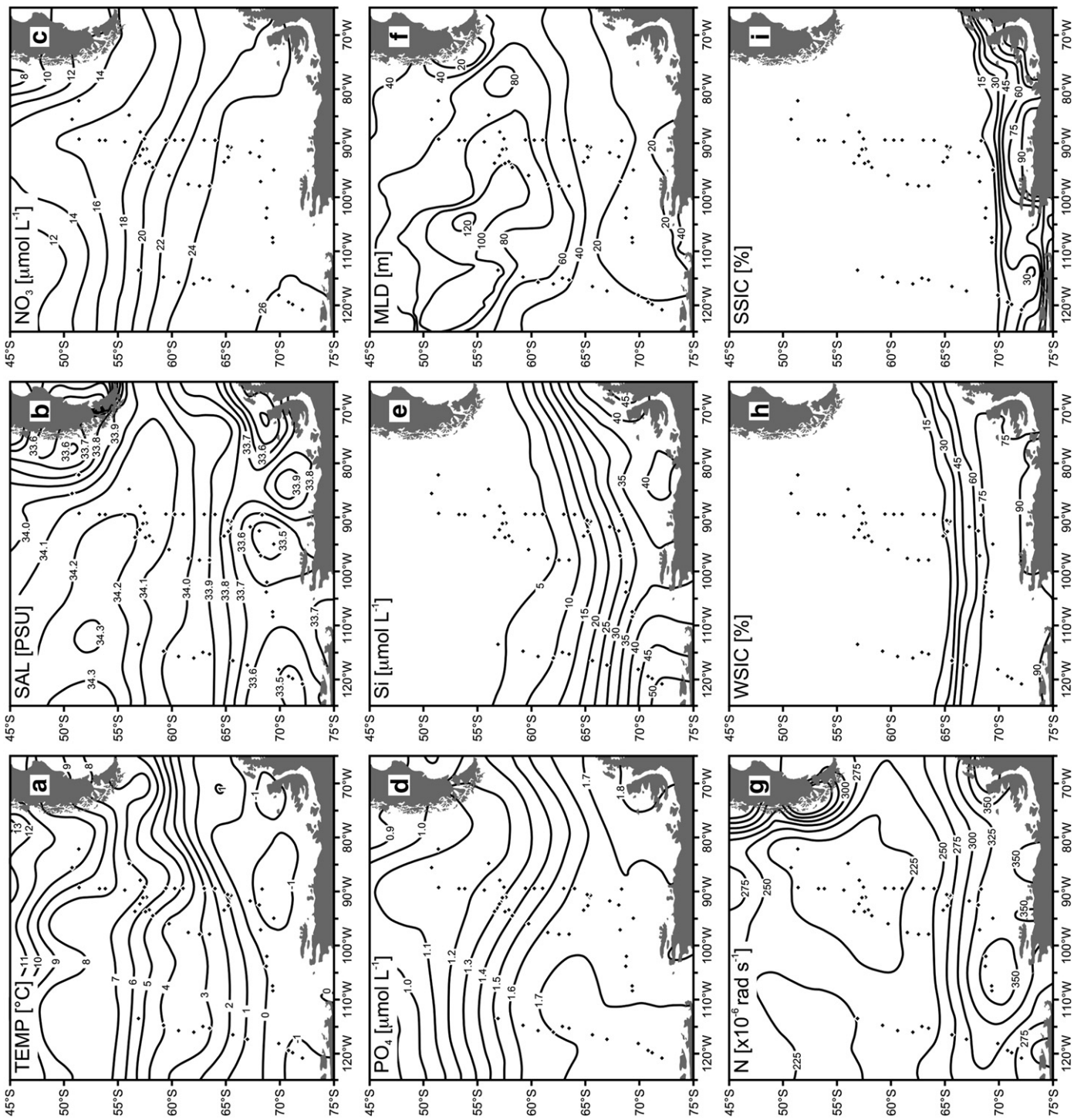

may be biased by selective dissolution (Burckle and Cirilli, 1987), the state of preservation of each sample was carefully determined. Our study relies on diatom species percent abundance, but also considers diatom valve accumulation rates. Comparison of diatom abundances with measured environmental variables (SST, salinity, nutrient concentrations, water column stability and sea ice concentration) relies on the results of statistical methods such as polynomial canonical redundancy analysis (polynomial RDA), to decipher the main environmental factors influencing the diatom species and their abundance distributions. We also compare the diatom assemblages preserved in the surface sediments with the results from plankton studies accomplished in the Pacific sector of the Southern Ocean. Such comparison is complicated by the fact that plankton net studies generally present "snap shot"-information from a specific season and the full range of diatoms including very weakly silicified species while surface sediment samples integrate assemblages deposited over years to decades or thousands of years and are biased towards more strongly silicified species due to selective dissolution. Nevertheless, phytoplankton studies from the Pacific sector (Kozlova, 1966; Hargraves, 1968; Hasle, 1969, 1976; Fenner et al., 1976; Kellogg and Kellogg, 1987; Burckle et al., 1987; Savidge et al., 1995) provide additional information on the autecological demands of the species preserved in the sediment record and can be used for a better understanding of environmental processes that steer the distribution of diatom species in the surface sediments.

2. Regional setting

The 52 studied surface sediment samples were recovered from the Amundsen and Bellingshausen Seas between 125°W–80°W and 75°S–50°S. The latitudinal coverage ranges from near-shore sites to the central Antarctic Circumpolar Current (ACC). The study area can be subdivided into four oceanographic zones, each characterised by specific hydrographic and nutrient regimes (Figs. 1 and 2). The southern boundary of the warmer (SSST ca. 7–14 °C) Subantarctic Zone (SAZ) is the Subantarctic Front (SAF), marked by distinct changes in temperature (ca. 4 °C) and salinity (ca. 0.22 PSU) (Lutjeharms and Valentine, 1984). The Polar Front Zone (PFZ) south of the SAF marks the northern limit of high nutrient regime typical of the Southern Ocean (Fig. 2). The PFZ is separated to its south by the Antarctic Polar Front (APF) from the Antarctic Zone (AZ), characterised by sea surface temperatures <4 °C and subsurface temperatures <2 °C. Highest Southern Ocean sea surface silicon concentrations occur in the AZ (Fig. 2). The AZ is divided from north to south into the Permanent Open Ocean Zone (POOZ), the Seasonal Sea Ice Zone (SSIZ) and the Sea Ice Zone (SIZ) close to the Antarctic coast. The SIZ is affected

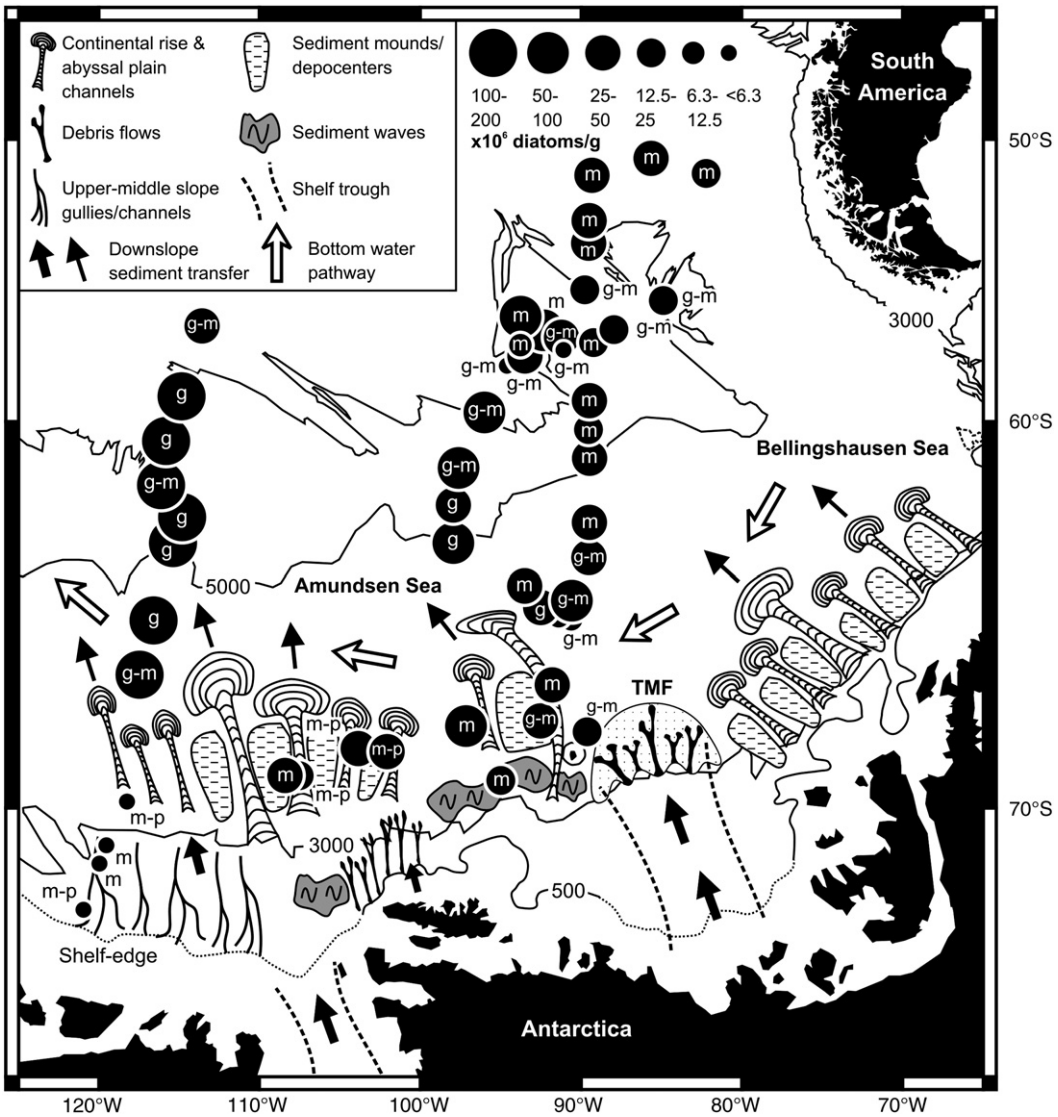

Fig. 3. Concentrations (valves/g) and preservation of the diatoms analysed in this study (preservation range: g = good, g–m = good–moderate, m = moderate, m–p = moderate–poor) in relation to the seafloor morphology in the Amundsen and Bellingshausen Seas (TMF: trough mouth fan; after Hillenbrand, 2000; Dowdeswell et al., 2006), and the bottom water pathways after Reid (1986). Bathymetric isolines (500, 3000, 5000) indicate the water depth in meters.

by winter and summer sea ice. Embedded in the AZ is the southern ACC Front (sACCF), which marks the southern boundary of the ACC. The location of this latter front is close to the maximum average winter sea ice extent (WSI; Fig. 1) (e.g. Armand and Leventer, 2003). A westwardly directed counter current occurs close to the Antarctic continent. The counter current´s bottom water component is assumed to consist mainly of Weddell Sea Deep Water generated in the Scotia Sea (Reid, 1986; Orsi et al., 1999; Scheuer et al., 2006; Rodehacke et al., 2007) (Fig. 3). While the northern part of the study area is characterised by less stratified surface waters with a deeper mixed layer, the southern region within the SSIZ and SIZ features stronger surface water stratification and a shallower mixed layer during summer.

The sedimentary environment varies from the heterogeneous area of the continental rise, characterised by sediment mounds, channels and debris flows to more homogeneous sediments of the abyssal plain below the ACC (Hillenbrand, 2000; Dowdeswell et al., 2006) (Fig. 3).

3. Material and methods

3.1. Material

Fifty-two surface sediment samples (Fig. 1; Table 1) were collected with a multicorer during AWI R/V *Polarstern* cruises ANT-XI/3, ANT-XII/4 and ANT-XVIII/5a (Miller and Grobe, 1996; http://www.pangaea.de/

Table 1
Station list and characteristics of the 52 analysed sediment samples.

Station [a]	Latitude	Longitude	Water depth (m)	Sediment type [b]	Bulk sediment AR ($g\ m^{-2}\ yr^{-1}$) [c]	BSi (%) [c]	BSi AR (mmol $m^{-2}\ yr^{-1}$) [c]	Total diatom counts	$\times 10^6$ Diatoms/g dry weight	Total diatom AR ($\times 10^8$ valves $m^{-2}\ yr^{-1}$)	Diatom preservation [d]
PS2546-1	72°03.12′S	120°55.77′W	2384	fbsm				56	0.5		m–p
PS2547-2	71°09.05′S	119°55.14′W	2092	fbsm				145	2.4		m
PS2548-2	70°47.38′S	119°30.43′W	2642	fbm				71	1.4		m
PS2550-2	69°51.53′S	118°13.00′W	3108	fbm				97	2.8		m–p
PS2657-1	51°21.90′S	82°13.20′W	4367	fbdm				548	17.5		m
PS2659-2*	50°44.94′S	85°41.28′W	4579	dbfm	2.5	10.2	3.9	599	38.4	0.97	m
PS2661-4*	51°24.54′S	89°20.70′W	4728	dbfm	2.6	9.5	3.7	520	41.5	1.08	m
PS2663-4*	53°17.22′S	89°32.82′W	4972	dm	1.9	16.1	4.7	486	25.9	0.50	m
PS2664-4*	53°49.14′S	89°34.86′W	4810	dm	1.4	19.4	4.1	474	37.9	0.53	m
PS2667-5*	55°39.12′S	89°4884′W	5531	dm	2.1	21.5	6.8	402	14.3	0.30	g–m
PS2668-1	57°16.62′S	91°15.06′W	4912	dm				487	31.1		g–m
PS2675-4	57°52.92′S	93°30.12′W	4914	fo				515	32.9		g–m
PS2676-1	58°13.02′S	94°34.80′W	3916	fo				477	4.2		g–m
PS2677-4	59°43.02′S	96°02.04′W	4698	dm				525	55.9		g–m
PS2678-2	61°30.00′S	97°41.10′W	5211	dm				510	81.5		g–m
PS2679-1	62°30.78′S	97°59.64′W	5142	dm				542	34.7		g
PS2680-4	63°27.18′S	98°00.06′W	5007	dm				719	52.2		g
PS2684-1*	69°25.02′S	95°01.44′W	4229	dm	4.7	9.0	6.3	455	21.8	1.02	m
PS2686-2	68°19.32′S	89°37.62′W	3953	dm				472	18.1		g–m
PS2687-5*	68°04.44′S	92°33.36′W	4454	dm	5.3	13.1	10.6	393	31.4	1.67	g–m
PS2688-4*	67°13.02′S	91°49.26′W	4627	dm	6.2	12.8	11.9	420	33.5	2.06	m
PS2690-1*	65°26.64′S	90°47.76′W	2404	dm	11.3	5.3	9.1	686	11.7	1.32	g–m
PS2691-1*	65°23.70′S	91°10.26′W	4715	dm	10.7	7.2	11.6	527	9.4	1.01	g–m
PS2692-1*	65°08.34′S	90°40.98′W	4674	dm	4.2	12.0	7.7	594	71.4	3.02	g–m
PS2694-1	64°48.72′S	93°34.80′W	4208	dm				451	27.7		m
PS2695-1	65°12.12′S	92°41.16′W	3316	dm				566	31.4		g
PS2696-4*	63°58.62′S	89°32.46′W	4768	dm	4.8	13.9	10.0	511	24.6	1.18	g–m
PS2697-1*	62°59.82′S	89°29.58′W	4783	dm	6.4	16.6	16.1	463	37.0	2.38	m
PS2699-5*	61°01.08′S	89°29.94′W	4957	dm	2.6	11.2	4.4	562	36.0	0.94	m
PS2700-5*	60°15.12′S	89°32.82′W	5012	dm	3.3	21.3	10.6	444	17.8	0.59	m
PS2701-2	59°26.46′S	89°30.36′W	4767	dm				440	35.3		m
PS2703-2	57°36.06′S	91°10.74′W	2746	dbfo				457	1.0		g–m
PS2714-6	57°26.76′S	89°16.26′W	5088	dm				459	12.6		m
PS2715-3*	57°02.46′S	88°00.48′W	5190	dm	2.4	18.9	7.0	466	18.8	0.46	g–m
PS2716-2*	56°01.26′S	84°54.30′W	5277	dm	1.8	21.0	5.8	415	16.0	0.29	g–m
PS58/252-1	68°11.20′S	97°09.30′W	4507	dbm				689	61.0		m
PS58/253-2*	69°18.50′S	107°33.70′W	3721	dbm	6.3	8.4	8.0	379	12.0	0.75	m–p
PS58/254-2	69°18.80′S	108°27.00′W	4016	fdbm				448	39.6		m
PS58/256-1*	68°42.70′S	103°53.80′W	4256	dbm	5.2	17.0	13.3	380	33.6	1.74	m–p
PS58/258-1	68°46.00′S	102°05.30′W	4181	dbm				415	36.7		m–p
PS58/265-1*	66°58.70′S	117°26.60′W	4600	do	4.9	54.4	40.3	376	167.3	8.16	g–m
PS58/266-4*	65°37.40′S	116°37.50′W	4845	do	5.5	72.4	60.8	816	181.5	10.06	g
PS58/268-1*	63°27.50′S	115°23.40′W	5099	do	5.4	63.0	51.2	596	175.9	9.45	g
PS58/269-4*	62°51.20′S	115°04.60′W	5087	do	6.0	75.6	69.1	402	118.7	7.16	g
PS58/270-1*	62°01.70′S	116°07.40′W	4982	do	5.0	75.3	56.6	700	155.7	7.72	g–m
PS58/272-4*	60°36.60′S	115°50.20′W	5078	do	5.7	80.0	69.5	629	185.5	10.65	g
PS58/274-4*	59°12.40′S	114°53.30′W	5135	do	4.3	75.1	49.3	623	138.0	5.97	g
PS58/276-1*	56°53.40′S	113°34.40′W	3896	fo	4.4	29.8	19.7	498	27.5	1.20	g–m
PS58/280-1*	57°32.70′S	93°49.70′W	4038	fo	4.9	9.0	6.7	472	7.0	0.34	m
PS58/290-1*	57°38.80′S	91°09.30′W	3341	do	10.0	2.6	3.9	442	5.6	0.56	g–m
PS58/291-3*	57°02.20′S	92°22.80′W	5026	fo	2.3	35.6	12.4	579	51.2	1.17	m
PS58/292-1*	56°34.00′S	93°47.60′W	5240	fo	2.2	30.0	10.1	425	75.2	1.66	m

[a] ANT-XI/3 (PS2546-1 to PS2550-2), ANT-XII/4 (PS2657-1 to PS2716-2), ANT-XVIII/5a (PS58/252-1 to PS58/292-1).
[b] dbfm: diatom bearing foraminiferal mud; dbfo: diatom bearing foraminiferal ooze; dbm: diatom bearing mud; dm: diatomaceous mud; do: diatomaceous ooze; fbdm: foraminifera bearing diatomaceous mud; fbm: foraminifera bearing. mud; fbsm: foraminifera bearing sandy mud; fdbm: foraminifera and diatom bearing mud; fo: foraminiferal ooze.
[c] For 31 samples (*) thorium corrected accumulation rates (AR) and opal (BSi) from Geibert et al. (2005) were used.
[d] Preservation range: g = good, g–m = good–moderate, m = moderate, m–p = moderate–poor.

PHP/CruiseReports.php?b=Polarstern; http://doi.pangaea.de/10.1594/PANGAEA.60007) and represent the topmost 0.5 cm of the sediment column.

Sample treatment and preparation of quantitative slides for light microscopy followed the standard procedure developed at the Alfred-Wegener-Institute (Gersonde and Zielinski, 2000), and the counting method is according to Schrader and Gersonde (1978). An average of 400–600 (minimum 379, maximum 816) diatom valves were counted per sample using a Zeiss Axioplan I microscope at ×1000 magnification. Exceptions to this count procedure were limited to four samples (PS2546-1, PS2547-2, PS2548-2, PS2550-2) recovered from the sea ice covered zone (according to Schweitzer, 1995) in the southwestern sector of the study area. In these four samples between 56 and 145 valves per sample were identified resulting in the lowest concentrations observed in the region ($<2.8\times10^6$ valves per g dry sediment).

The preservation state of the diatom samples was noted because it provided additional information in assessing the robustness of the observed sedimentary distributions, as selective diatom preservation may bias the reference data set. Three stages of preservation were distinguished following the definition proposed by Zielinski (1993). The categories are:

Good (g): assemblage consists of mixture of heavily and delicately silicified species, no enlargement of the areolae or dissolution at the valve margin can be detected.

Moderate (m): heavy and delicately silicified species are present, with the delicately silicified species showing areolae enlargement, dissolution of the valve margin and valve fragmentation.

Poor (p): predominantly heavily silicified species, strong dissolution of the valve margin and enlargement of areolae, fractionation of valves due to dissolution.

The diatom data set is available on request from the Pangaea database (http://doi.pangaea.de/10.1594/PANGAEA.681699).

Out of the 52 samples, 31 were previously analysed for ^{230}Th-excess and biogenic silica (BSi) content (Geibert et al., 2005; data available at http://doi:10.1594/PANGAEA.230042), allowing for the calculation of diatom valve accumulation rates (AR) of specific species and species groups and its comparison with the BSi content and the BSi AR. Although no absolute ages for the sediment samples are available the biogenic particles of the sediments analysed are considered to be of modern origin (Geibert et al., 2005).

3.2. Data preparation and selection

Diatoms were generally identified to species or species group level and, if applicable, to variety or forma level. Following the taxonomy described by Hasle and Syvertsen (1996), Zielinski and Gersonde (1997) and Armand and Zielinski (2001) we identified 33 species, 7 varieties and 3 forma (see Appendix A for taxonomic details). Some taxa were combined as groups according to Zielinski and Gersonde (1997). For simplicity we summarise these different taxa in this paper under the general terms species and species groups.

Chaetoceros vegetative valves and spores were included in one group, named *Chaetoceros* spp. The observed *Chaetoceros* specimens belong exclusively to the subgenus *Hyalochaetae*, mainly represented by resting spores. Distinguishing resting spores from vegetative valves was not possible; in most of the preserved valves it was impossible to identify the presence of setae, one feature characterising vegetative valves. For the same reason it was also not possible to identify the *Chaetoceros* specimens to species level.

Due to the varying preservation of the *Eucampia* frustules in the analysed samples, the two varieties *Eucampia antarctica* var. *antarctica* and *E. antarctica* var. *recta* could not clearly be separated and were combined in the *Eucampia antarctica* group.

The *Thalassionema nitzschioides* group combines *T. nitzschioides* var. *lanceolata* and *T. nitzschioides* var. *capitulata*, two varieties with a gradual transition of features between them.

In the *Thalassiosira gracilis* group, *T. gracilis* var. *gracilis* and *T. gracilis* var. *expecta* were combined. The appearance of gradual transitions between both varieties made a consistent separation between the two varieties impossible. Furthermore, the geographic distribution of the two varieties showed no discernible pattern, i.e. *T. gracilis* var. *expecta* occurred only sporadically in 4 samples and was never represented by more than two specimens per sample.

Of the 41 species and species groups identified, 27 were selected for statistical analysis (Table 2; Appendix C). The 14 excluded species, each with a cumulative relative abundance of less than 1% in all 52 samples and/or a scattered distribution pattern, were not considered for these reasons.

Relative abundance plots of 26 selected species and species groups in relation to the mean summer sea surface temperature are provided in Fig. 4. Eighteen prominent species and species groups were plotted on the basis of their common distribution in the study area. The biogeographic analysis and subsequent statistical analysis of species with respect to environmental variables was initially undertaken on all samples recovered, whereas the analyses of accumulation rates were undertaken on two latitudinal transects, one with 10 samples around 120°W from 55°S to 70°S (referred to below as the western transect) and the second with 21 samples around 90°W from 50°S to 70°S (the eastern transect).

3.3. Data processing

The raw counts were transformed to relative abundances in order to map the diatom distributions. A further logarithm-based transformation was performed as a prerequisite of the canonical redundancy analysis using the following equation:

$$Y = LOG_{10}(\textit{relative abundance} \times 10 + 1) \quad (1)$$

The determination of species accumulation rates (AR) was calculated using two equations. First, the diatom valve concentration per gram dry sediment was calculated:

$$\textit{Diatom valves}/g = (1/wt) \times (csp/tp) \times (susp/split) \times (\textit{diatom valve number}/traverse), \quad (2)$$

where *wt* is the dried sample weight in grams, *csp* is the cover slip area (254.5 mm^2), *tp* is the area of the counted traverse (4.5 mm^2), *susp* is the initial volume of processed diatom suspension (55 ml), *split* is the volume of suspension pipetted onto the cover slip (from 6.5×10^{-3} to 4.9×10^{-1} ml) and *traverse* is the number of traverses fully counted under the light microscope (from 1 to 10).

The results of Eq. (2) were then multiplied with the bulk sedimentary accumulation rate (AR) previously determined from thorium isotopes (Geibert et al., 2005):

$$\textit{Diatom valve AR}\,[\textit{diatom valves}\ m^{-2}yr^{-1}] = \textit{diatom valves}/g \times \textit{bulk AR}[g\ m^{-2}yr^{-1}], \quad (3)$$

resulting in total diatom valve AR and values for specific species and species groups for the 31 samples (Table 1) along the two transects. For the 18 more prominent species and species groups the AR were compared to the oceanic frontal system and the maximum average summer and winter sea ice concentrations along both transects.

3.4. Statistical methodology

To determine which environmental gradients in the upper water column might influence the spatial distribution of the diatoms in the sediments, the statistical method of polynomial canonical redundancy analysis (RDA) was applied to the diatom´s logarithm-transformed

Table 2
Fourty-one diatom species/species groups and their relation to sea surface temperatures.

Name	Abbrev.	Range of abundance (%)	SSST range (°C) this study[#]	SSST range (°C) from literature [a, b, c, d]
*Actinocyclus actinochilus**	Aacti	0–11.0	−1.5 to 0	−2 to 2[a], −1.3 to 9[b]
A. curvatulus	Acurv	0–0.4		
*Asteromphalus hookeri**	Ahook	0–0.6		
A. hyalinus	Ahyal	0–0.5		
*A. parvulus**	Aparv	0–1.4		
*Azpeitia tabularis var. egregius**	Ataeg	0–9.7	6–10	
A. tabularis var. *tabularis**	Atata	0–13.4	−0.5 to 10	0–20[a], 11–22.3[b]
Chaetoceros spp.*	Chaet	0–8.3	−1.5 to 10	−2 to 12[a], −1.3 to 3.5[b]
*Eucampia antarctica**	Eanta	0–12.5	−1.5 to 7	−2 to 12[a]
*Fragilariopsis curta**	Fcurt	0–17.9	−1.5 to 3	−2 to 2[a], −1.3 to 2.5[b]
*F. cylindrus**	Fcyli	0–2.1	−1.5 to 0	−2 to 2[a], −1.3 to 3[b]
F. doliolus	Fdoli	0–0.2		8 to 20[a], 10.5–22.3[d]
*F. kerguelensis**	Fkerg	35–85	−1 to 10	−1 to 18[a], −1 to 22[c]
*F. obliquecostata**	Fobli	0–0.3	−0.5 to 6	−2 to 0.5[a], −1.3 to 2[b]
*F. rhombica**	Frhom	0–2.2	−0.5 to 6	−2 to 5[a], −1.3 to 11.5[b]
*F. ritscheri**	Frits	0–1.7	−0.5 to 1	−2 to 5[a], −1.3 to 7.5[b]
*F. separanda**	Fsepa	0–7.3	−1.5 to 7	−1.5 to 12[a], −1.3 to 8[b]
F. sublinearis	Fsubl	0–1.6	0	−2 to 1[a], −1.3 to 2.5[b]
*Hemidiscus cuneiformis**	Hcune	0–2.4	8–10	7.5–20[a], 8.5–22.3[d]
Nitzschia bicapitata	Nbica	0–0.4		5–20[a]
N. kolaczeckii	Nkola	0–0.2		
Porosira glacialis	Pglac	0–0.2		−2 to 1.5[a], −1.3 to 2[b]
Pseudo-nitzschia turgiduloides	Pturg	0–0.7		−2 to 1[a]
Rhizosolenia species A*	RspA	0–0.7		−1 to 12[a]
R. antennata forma *antennata*	Ranan	0–0.3		11 to 20[a]
R. antennata f. *semispina**	Ranse	0–0.2		−1 to 19[c]
*R. bergonii**	Rberg	0–0.7		
*Roperia tesselata**	Rtess	0–4.4	5–10	4–20[a], 6.5–22.3[d]
Thalassionema nitzschioides f. 1*	Tnif1	0–0.5		0–20[a]
T. nitzschioides group*	Tnigr	0–3.6	2–10	2–20 [a], 2–19[c]
T. nitzschioides var. *parva*	Tnipa	0–0.4		13–20[a], 8.5–20[d]
Thalassiosira antarctica	Tanta	0–0.2		−2 to 9.5[a], −1.3 to 3.5[b]
T. frenguelliopsis	Tfren	0–0.3		
*T. gracilis**	Tgrac	0–12.3	−1.5 to 7	−2 to 13[a], −1.3 to 18[c]
T. gravida	Tgrav	0–0.2		
*T. lentiginosa**	Tlent	2.1–29.7	−1.5 to 10	−1 to 16[a], −0.5 to 18[c]
*T. oestrupii**	Toest	0–1.5	1–10	5–20[a], 4.5–22.3[d]
*T. oliverana**	Toliv	0–2.7	−0.5 to 6	−1.5 to 5 , −1.3 to 18[c]
*T. trifulta**	Ttrif	0–0.7		
T. tumida	Ttumi	0–0.2		−1.3 to 7[b]
*Thalassiothrix antarctica**	Txant	0–5.0	−1 to 10	−2 to 20[a], −0.5 to 18[c]

*Twenty-seven species/species groups used for the statistical analysis.
#A temperature range is given only for species/species groups with a maximum relative abundance >1.5%.
[a]Zielinski and Gersonde (1997) – Atlantic sector; [b]Armand et al. (2005), [c]Crosta et al. (2005),
[d]Romero et al. (2005) – Atlantic and Indian sectors.

relative abundances using the computer software PolyRDA-CCA (polynomial redundancy analysis-canonical correspondence analysis; Makarenkov and Legendre, 2002). This method was chosen over the R- and Q-mode factor analyses used in similar Southern Ocean studies (e.g. Cunningham and Leventer, 1998; Zielinski et al., 1998; reviewed in Armand and Leventer, 2009). Instead of revealing regional factors controlling diatom assemblage distributions, polynomial RDA directly relates diatom species and species group distribution to different environmental variables. Polynomial RDA is able to relate more of the variance in the diatom data set to environmental variation than linear RDA, a method well known from recent palaeoecological studies (e.g. Birks, 1998; Radi et al., 2007; Richter et al., 2007). Here, the species and species group arrangements in a biplot can be directly related to known environmental conditions of the overlying surface waters through the use of RDA. In this case, the length of the arrow representing a known variable is a function of that variable's importance in determining the species variation. Species that plot close to the centre of the diagram (i.e. have short lines) show no significant abundance variation within the data set. The correlation coefficient between a species and the environmental gradient corresponds to the cosine of the angle between the species line and that of the gradient: a positive score represents increasing abundance of a species along the gradient and a negative score, the reverse. Linear RDA is based on the assumption that species show a linear response to changing environmental gradients, i.e. increase or decrease in abundance linearly along an increasing environmental gradient such as the spatial temperature variation. Polynomial RDA assumes a non-linear relationship between the response variables (species) and the explanatory variables (environmental variables). Makarenkov and Legendre (2002) state: "There is no special reason why nature should linearly relate changes in species assemblages to changes in environmental variables." Moreover, the use of the new technique of polynomial RDA produces a noticeable increase in the amount of total variability accounted for within the response variables compared to linear RDA (comparison not shown). For this reason we report our findings for environmental forcing on the abundance distributions based on the polynomial RDA technique.

The environmental variable data set (Table 3) comprised: the mean summer sea surface temperatures and salinities (TEMP and SAL; at 10 m water depth; Fig. 2a,b) from the WOCE Global Hydrographic Climatology-Atlas (Gouretski and Koltermann, 2004); the mean annual sea surface concentration (at 10 m water depth) of dissolved

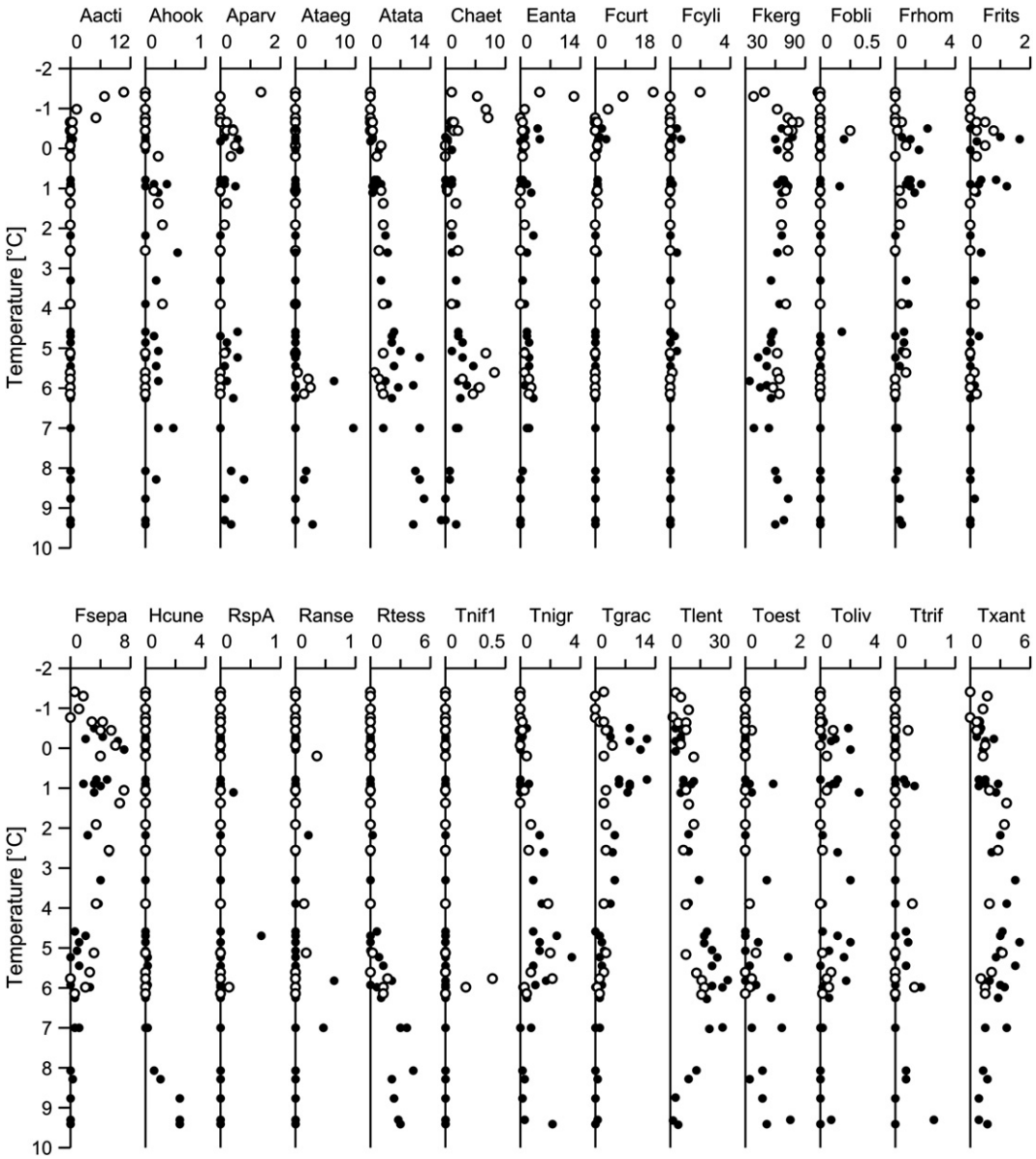

Fig. 4. Relative abundances of the 26 diatom species and species groups used in the statistical analysis. Open circles represent samples from the western sector of the study area, closed circles represent samples from the eastern sector (sectors are divided by the 100°W meridian). For diatom name abbreviations see Table 2.

nitrate (NO_3; Fig. 2c), phosphate (PO_4; Fig. 2d) and silicon (Si; Fig. 2e) obtained from the World Ocean Atlas 2005 (Garcia et al., 2006); and two variables reflecting the surface water structure, the mean mixed layer depth in summer (MLD; Fig. 2f) and the mean annual water density between 0 m and 75 m depth gained from the LEVITUS94 World Ocean Atlas (Monterey and Levitus, 1997). The variable N (in rad s^{-1}) represents the mean annual Brunt–Väisälä-frequency for each station, calculated from water densities as a measure of the stratification of the upper water column between 0 m and 75 m water depth (after Vink, 2004):

$$N = \sqrt{(9.8 \times \delta D) / (1026 \times \delta z)},$$

where δD represents the density difference over the distance δz (in this case 75 m, at which the depth interval covers the range of summer MLD variation). Higher values of N represent increased stratification (Fig. 2g). Finally the mean winter (WSIC; Fig. 2h) and summer (SSIC; Fig. 2i) sea ice concentrations (Schweitzer, 1995) were used to determine the influence of sea ice on the species distribution.

4. Results

4.1. Diatom occurrence and species distribution pattern

Highest diatom concentrations in surface sediments (up to 185×10^6 valves/g dry sediment) and best preservation occured in the western and central part of the study area, approximately between the SAF and the southern ACC-boundary (Fig. 3, Table 1). In contrast, the samples from the continental slope of the Amundsen Sea were characterised by mid-ranging diatom concentrations ($10–40 \times 10^6$ valves/g dry sediment) and moderate preservation. The continental slope is affected by channeling and multiple debris flows and turbidites (Fig. 3). The lowest diatom concentrations ($0.5–3 \times 10^6$ valves/g dry sediment) and moderate to poor diatom preservation occurred at four sample sites, all located in the southwestern sector of the study area, which is affected by year-round sea ice cover (Fig. 2i). North of the SAF, diatom concentrations were also low to mid-ranging ($20–40 \times 10^6$ valves/g dry sediment; Fig. 3). Here, diatom preservation was generally observed as moderate. The distribution pattern of diatom valve concentration was mirrored by the diatom valve ARs,

Table 3
Environmental variables used in the statistical analysis.

Station	Temperature [a] (°C)	Salinity [a] (p.s.u)	Nitrate concentration (μmol L^{-1}) [b]	Phosphate concentration (μmol L−[1]) [b]	Silicon concentration (μmol L^{-1}) [b]	Mixed layer depth (m) [c]	Brunt–Väisälä-frequency ($\times 10^{-6}$ rad s^{-1}) [c]	Summer sea ice concentration (%) [d]	Winter sea ice concentration (%) [d]
PS2546-1	−1.28	33.58	23.95	1.46	61.86	14.68	256.74	54	87
PS2547-2	−1.37	33.56	23.87	1.58	60.37	12.89	279.29	31	84
PS2548-2	−0.93	33.55	23.93	1.62	59.25	12.83	295.43	31	84
PS2550-2	−0.75	33.53	24.21	1.68	55.44	12.87	308.61	31	84
PS2657-1	9.45	34.05	13.68	1.26	3.86	47.95	203.32	0	0
PS2659-2	9.33	34.07	16.33	1.23	4.86	58.31	222.01	0	0
PS2661-4	8.78	34.12	16.75	1.16	3.74	64.97	221.20	0	0
PS2663-4	8.29	34.14	16.35	1.16	2.93	79.43	215.38	0	0
PS2664-4	8.07	34.15	16.37	1.16	2.78	83.02	215.38	0	0
PS2667-5	7.01	34.15	16.88	1.19	2.34	91.75	212.88	0	0
PS2668-1	5.97	34.12	18.23	1.29	2.44	92.70	214.41	0	0
PS2675-4	5.48	34.10	19.23	1.36	2.89	88.37	215.47	0	0
PS2676-1	5.26	34.09	19.83	1.40	3.33	81.68	217.53	0	0
PS2677-4	4.60	34.06	21.07	1.47	4.89	70.11	220.49	0	0
PS2678-2	3.91	34.00	22.57	1.55	7.85	50.81	228.17	0	0
PS2679-1	3.33	33.93	23.40	1.59	9.47	43.62	234.08	0	0
PS2680-4	2.62	33.83	24.03	1.61	10.85	38.17	243.19	0	0
PS2684-1	−0.48	33.40	25.00	1.69	35.95	7.03	345.05	0	79
PS2686-2	−0.20	33.51	25.39	1.68	32.89	10.93	330.09	24	80
PS2687-5	−0.16	33.47	24.71	1.64	26.71	10.98	334.25	3	81
PS2688-4	0.09	33.50	24.46	1.61	21.52	13.50	316.86	0	49
PS2690-1	0.81	33.60	24.41	1.59	14.73	23.22	272.49	0	17
PS2691-1	0.84	33.60	24.41	1.60	14.49	23.49	274.07	0	17
PS2692-1	0.94	33.62	24.43	1.60	14.20	25.86	272.49	0	17
PS2694-1	1.15	33.64	24.55	1.61	12.81	29.74	257.28	0	14
PS2695-1	0.96	33.61	24.46	1.60	13.73	25.03	275.20	0	14
PS2696-4	0.93	33.70	24.39	1.59	12.25	43.08	238.76	0	1
PS2697-1	2.19	33.83	24.00	1.57	10.35	57.91	238.76	0	1
PS2699-5	4.70	34.05	22.01	1.48	6.25	74.10	224.76	0	0
PS2700-5	4.88	34.07	21.07	1.44	4.96	78.72	220.71	0	0
PS2701-2	5.09	34.09	19.92	1.38	3.72	83.55	217.80	0	0
PS2703-2	5.83	34.12	18.39	1.30	2.49	92.33	214.41	0	0
PS2714-6	6.00	34.13	17.85	1.26	2.37	91.02	214.25	0	0
PS2715-3	6.28	34.13	17.32	1.24	2.33	89.44	214.89	0	0
PS2716-2	7.04	34.14	16.39	1.23	2.77	83.76	217.44	0	0
PS58/252-1	−0.27	33.38	24.02	1.58	22.59	8.51	338.19	0	76
PS58/253-2	−0.62	33.43	25.53	1.67	43.36	4.42	364.73	1	81
PS58/254-2	−0.63	33.44	25.56	1.68	44.54	4.95	362.10	1	81
PS58/256-1	−0.44	33.41	24.74	1.60	31.70	4.54	355.48	0	81
PS58/258-1	−0.43	33.40	24.42	1.57	28.32	4.83	353.37	0	81
PS58/265-1	−0.07	33.58	24.51	1.72	38.74	19.89	285.69	0	67
PS58/266-4	0.25	33.62	24.63	1.73	28.90	25.32	267.17	0	13
PS58/268-1	1.08	33.74	24.60	1.72	15.89	35.16	238.18	0	0
PS58/269-4	1.41	33.75	24.46	1.70	13.05	40.84	231.60	0	0
PS58/270-1	1.92	33.82	24.08	1.63	11.64	43.54	234.03	0	0
PS58/272-4	2.57	33.97	23.34	1.54	7.62	46.53	228.05	0	0
PS58/274-4	3.94	34.05	22.27	1.46	5.14	52.46	227.43	0	0
PS58/276-1	5.17	34.13	19.65	1.34	3.10	54.12	224.71	0	0
PS58/280-1	5.64	34.11	19.06	1.35	2.81	87.64	215.47	0	0
PS58/290-1	5.81	34.12	18.41	1.30	2.50	92.24	214.41	0	0
PS58/291-3	6.02	34.13	18.31	1.29	2.49	92.36	214.89	0	0
PS58/292-1	6.18	34.13	18.23	1.29	2.55	86.64	214.61	0	0

[a] Sea surface (10 m water depth) summer temperature and salinity taken from the WOCE Global Hydrographic. Climatology Atlas (Gouretski and Koltermann, 2004).
[b] Mean annual sea surface (10 m water depth) concentration of dissolved nitrate, phosphate and silicon; variables derived from the World Ocean Atlas 2005 (Garcia et al., 2006).
[c] Mixed layer depth in summer and the Brunt–Väisälä-frequency (*N*) calculated from the mean annual water density from water depth of 0 m and 75 m; data from the LEVITUS 94 World Ocean Atlas (Monterey and Levitus, 1997).
[d] Winter (WSI) and summer (SSI) sea ice concentrations after Schweitzer (1995).

calculated on the basis of ^{230}Th-normalised flux rates from Geibert et al. (2005). The diatom valve ARs obtained from the western transect were generally one order of magnitude higher than those from the eastern transect (Fig. 5a,b). Highest values ($8–10\times10^8$ valves m^{-2} yr^{-1}) were encountered around 120°W between the SAF and the northern SSIZ, extending over ca. 900 km between 60°S and 68°S (Fig. 5a). This pattern is mirrored by the BSi content of the sediment and the BSi ARs, reaching maximum values between 70–80% and around 60 mmol m^{-2} yr^{-1}, respectively (Fig. 5c,e). The latitudinal pattern of diatom valve ARs obtained from the eastern transect is less clear and this also accounts for the BSi content and its accumulation rates (Fig. 5b,d,f). Highest diatom valve ARs (around 20×10^7 valves m^{-2} yr^{-1}) have been encountered between 62°S and 68°S, which is south of the APF and north of the maximum mean summer sea ice extent (SSI), respectively. This is similar to the pattern of the BSi accumulation (around 12 mmol m^{-2} yr^{-1}), while the BSi values only reach around 15% of the total sediment content. A distinct peak in all three parameters occurs north of the SAF, with diatom AR around 12×10^7 valves m^{-2} yr^{-1}, BSi content around 30% and BSi ARs around 10 mmol m^{-2} yr^{-1}.

In the following paragraph, the biogeographic distribution of 18 selected diatom species and species groups and the accumulation rate (AR) pattern along the western and eastern transects are described in alphabetical order. The observed summer sea surface temperature

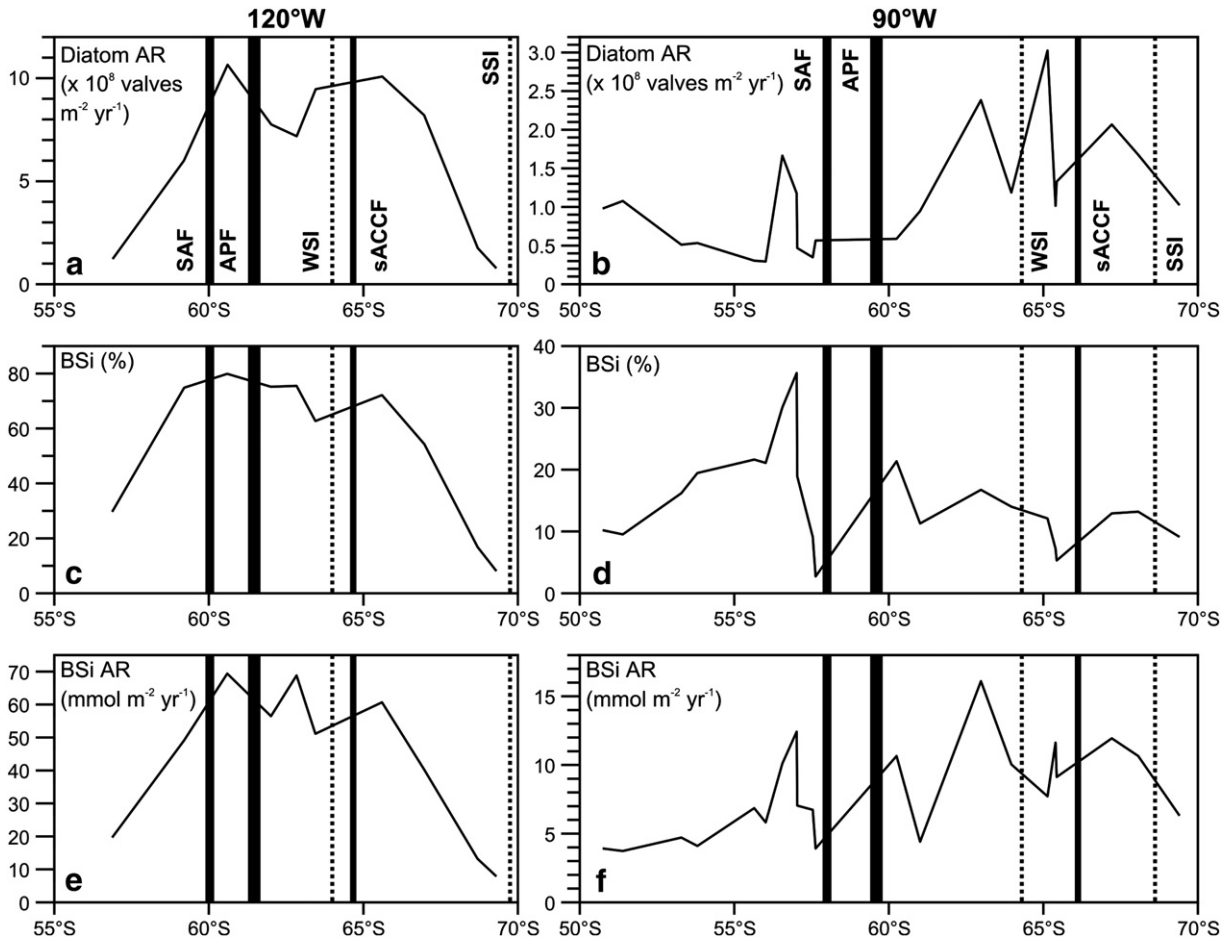

Fig. 5. Total diatom accumulation rates (diatom valve AR; plots a,b), biogenic opal relative abundance (BSi; from Geibert et al., 2005; plots c, d) and biogenic opal accumulation rates (BSi AR; from Geibert et al., 2005; plots e, f) compared between the 120°W and the 90°W transects. Abbreviations: APF: Antarctic Polar Front; sACCF: southern ACC Front; SAF: Subantarctic Front; SSI: maximum average summer sea ice extent; WSI: maximum average winter sea ice extent.

(SSST) ranges for each species and species group are summarised in Table 2.

Actinocyclus actinochilus displayed significant relative abundances at the southernmost sites, an area on the western transect that is affected by year-round sea ice (Figs. 2h,i and 6a). Average summer sea surface temperatures (SSST) in this area ranged between −1.5 and 0 °C (Fig. 2a).

Azpeitia tabularis var. *egregius* was only encountered along the eastern transect. Higher abundances were restricted to an area north of the SAF, at SSST around 6 °C (Figs. 4 and 6d,e).

Azpeitia tabularis var. *tabularis* displayed a broader zone of occurrence than its variety *egregius*. Amounts >5% of the total assemblages occurred between SSSTs of 10 °C in the SAZ and 2 °C (POOZ) in the study area and maximum values were centred around 9 °C (Fig. 7a). Southernmost occurrences were observed in the SSIZ (Fig. 7a). At the western transect the *A. tabularis* var. *tabularis* AR mirrored the pattern of the total diatom valve AR as a result of the lack of a latitudinal abundance gradient (Fig. 7b). Such a gradient occurred in the eastern transect and led to the highest species AR values in its northern section (Fig. 7c).

Relative abundances of the *Chaetoceros* spp. group revealed a bimodal distribution pattern with occurrences >5% south of the SSI (SSST around −1 °C) and north of the SAF at SSST around 6 °C (Figs. 2a,i, and 7d).

The Eucampia antarctica group has been encountered over a large environmental range. Highest relative abundances (>5%) occurred in the area affected by winter and summer sea ice, but also at sites north of the SAF (SSST 6–7 °C) where around 3% of the preserved diatom assemblages consisted of the *E. antarctica* group (Figs. 2 and 8a).

The archetypal sea ice indicator species, *Fragilariopsis curta* (Gersonde and Zielinski, 2000; Armand et al., 2005) displayed abundances >2% of the total diatom assemblage. The species was restricted to the southernmost study area, where sea ice cover is near annually persistent (Figs. 2 and 8d). Low abundances (<1%) have been observed as far north as the area of the SAF (Fig. 8d). Consequently the ARs calculated for *F. curta* show a clear S–N gradient in both transects (Fig. 8e,f).

Fragilariopsis kerguelensis represents the most dominant species in the study area. Except for the southernmost sample site (PS2546-1) and four sites located in the southernmost SAZ (eastern transect), *F. kerguelensis* contributes >50% to the assemblages (Fig. 9a). Consequently the pattern of the *F. kerguelensis* ARs clearly reflects the total diatom valve and the BSi ARs (Figs. 5 and 9b,c). At the western transect *F. kerguelensis* ARs reached highest values ranging between 5 and 8×10^8 valves $m^{-2}\,yr^{-1}$ in the zone of highest BSi deposition. This makes *F. kerguelensis* valves the major contributor to the BSi preserved at the sea floor.

Fragilariopsis rhombica and *Fragilariopsis ritscheri* occurred poorly across the two transects. Highest abundances and species ARs were noted in samples from the eastern transect specifically in between the mean SSI and WSI boundaries (Figs. 9d,f and 10a,c).

The relative abundance distribution of *Fragilariopsis separanda* clearly shows a N–S increase from the SAZ to the SSIZ. Overall higher relative abundances occurred in the western sector of the POOZ. Lowest relative abundances occurred at the southernmost sample sites (western transect), located in an area affected by winter and summer sea ice, and at the northernmost sites (eastern transect),

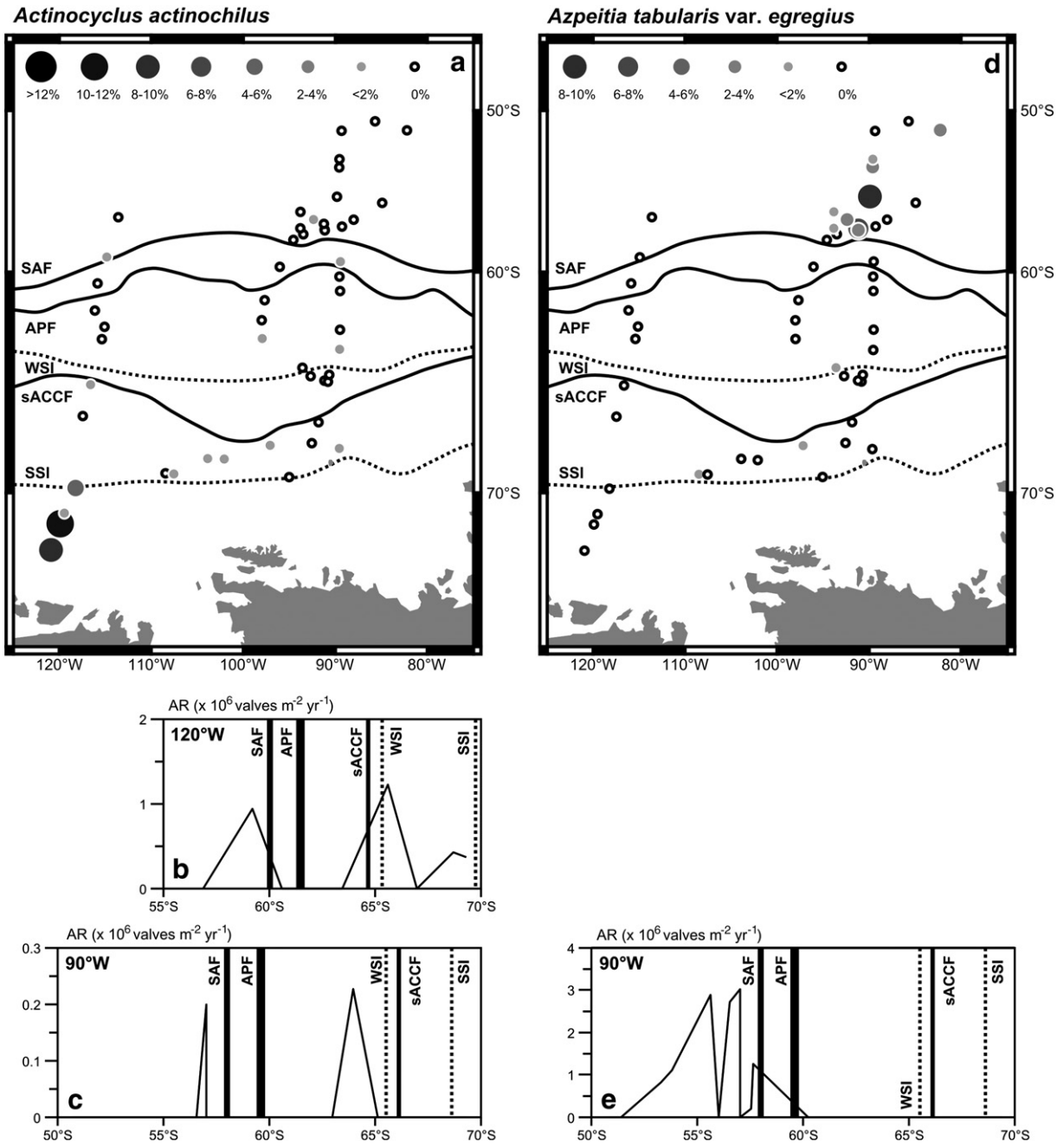

Fig. 6. Relative abundance maps and valve accumulation rates (AR) of the diatom species *Actinocyclus actinochilus* (a, b, c) and *Azpeitia tabularis* var. *egregius* (d, e). Abbreviations: APF: Antarctic Polar Front; sACCF: southern ACC Front; SAF: Subantarctic Front; SSI: maximum average summer sea ice extent; WSI: maximum average winter sea ice extent.

where SSST>8 °C. Maximum abundances and valve ARs occurred in the POOZ and the SSIZ where SSSTs range between 0 and 4 °C (Figs. 2a and 10d,e,f).

The typical warm water species *Hemidiscus cuneiformis* (Zielinski and Gersonde, 1997; Romero et al., 2005) was present exclusively at northernmost sample sites (eastern transect), where SSSTs were >8° (Figs. 4 and 11a,b).

Roperia tesselata, another warm water species (Zielinski and Gersonde, 1997; Romero et al., 2005), showed a larger range of distribution, extending as far south as the SAF (Fig. 11c,d,e). Highest abundances were referable to SSSTs>7 °C.

The *Thalassionema nitzschioides* group exhibited greatest abundances north of 64°S (SSST >3 °C) and the influence of the seasonal sea ice (Figs. 4 and 12a,b,c). Along the western transect, highest ARs occurred north of the APF, whereas along the eastern transect a comparably lower AR maximum occurred south of the APF.

The *Thalassiosira gracilis* group displayed highest relative abundances in the southern section of the eastern transect, at SSSTs between −1 and 1 °C (Fig. 4). In the western transect, relative abundances were comparably lower than in the east (Fig. 12d), but ARs along 120°W were higher compared to the 90°W transect, with a broader distribution range from the southern SAZ to the SSIZ. Maximum ARs occurred along both transects in the SSIZ between WSI and SSI. (Fig. 12e,f).

Thalassiosira lentiginosa showed highest relative abundance at the eastern transect between the Antarctic Zone and the SAZ, which corresponds to a SSST range from 4 to 8 °C. The zone of high *T. lentiginosa* ARs expands further southward to about 65°S where SSST are 2 °C (Figs. 2a and 13a,b,c). The rather large and strongly

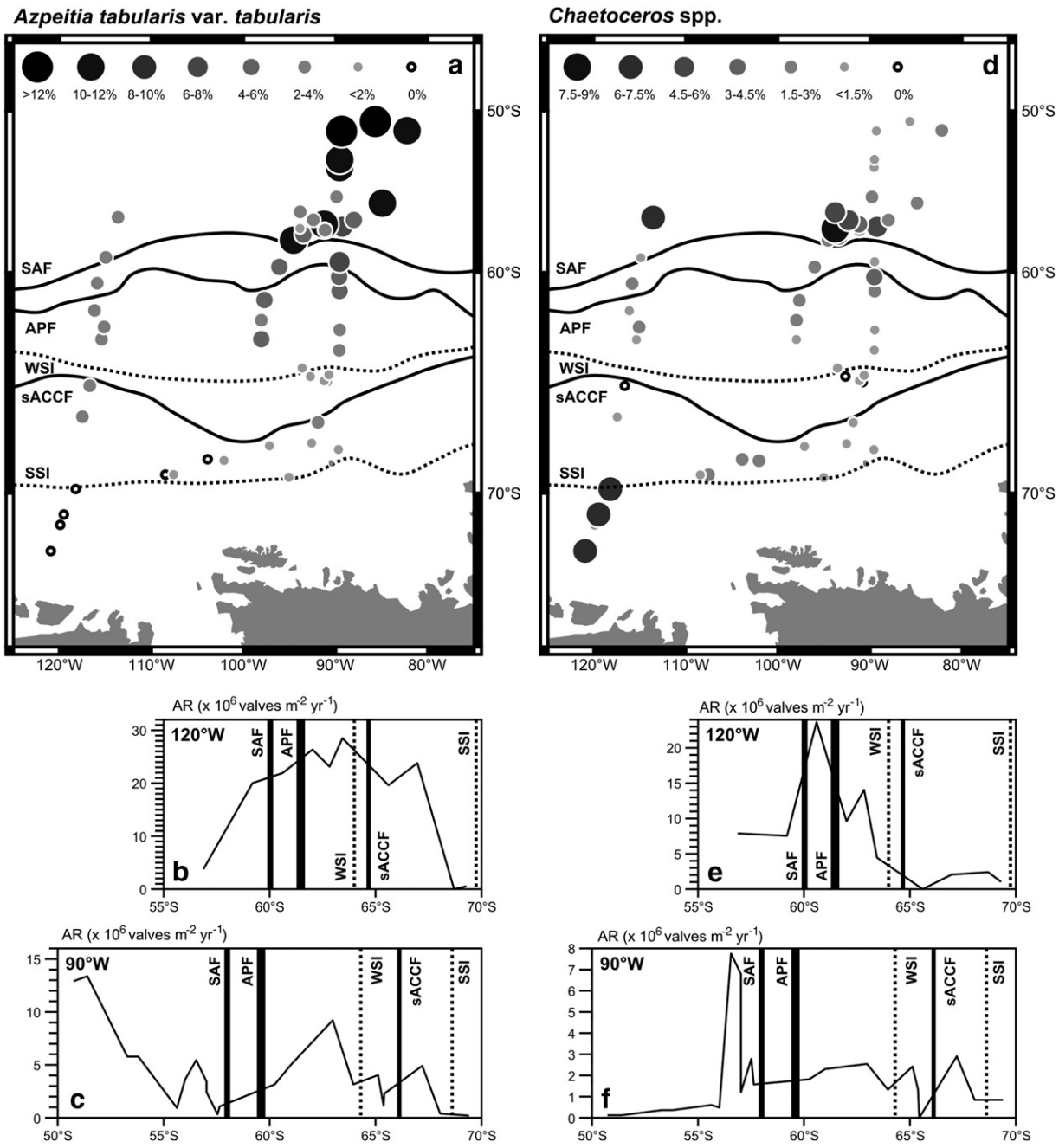

Fig. 7. Relative abundance maps and valve accumulation rates (AR) of the diatom species/species groups *Azpeitia tabularis* var. tabularis (a, b, c) and *Chaetoceros* spp. (d, e, f). Abbreviations as in Fig. 6.

silicified valves of *T. lentiginosa* represent another prominent contributor to the total diatom AR (Fig. 5a,b), inclusive of BSi % content at the sea floor (Fig. 5c,d), and the BSi AR latitudinal trends (Fig. 5e,f).

Thalassiosira oestrupii war encountered only rarely (<1.5% relative abundance; Table 2) Their dominance and highest AR values were found north of the SAF, where SSSTs are >5 °C (Figs. 2a and 13d,e,f).

The heavily silicified *Thalassiosira oliverana* exhibited higher relative abundances and valve ARs in the AZ along the eastern transect (SSSTs −0.5 to 4 °C; Figs. 2a and 14a,b,c). This species revealed trace occurrence in the western transect (Fig. 14a).

The needle-shaped *Thalassiothrix antarctica* was encountered at all sample sites, with exception to two southerly sites in the western transect affected by summer sea ice (Fig. 14d). The species abundances were greatest in the southern SAZ and POOZ across both transects, where SSSTs ranged between 3 and 8 °C (Figs. 4 and 14d).

The remaining 23 species and species groups preserved in the studied set of samples showed no distinct distributional patterns due to their low relative abundances, and resulted in negligible contributions to the total diatom accumulation rates (not shown). Regardless of the poor representation of certain species encountered, some of these species contribute to the variance in assemblage composition within the polynomial RDA. These species are: *Fragilariopsis cylindrus*, *Fragilariopsis ritscheri* and *Thalassiosira trifulta*.

4.2. Polynomial canonical redundancy analysis (polynomial RDA)

The statistical analysis of 27 selected species and species groups from the 52 samples (Table 2) via the polynomial RDA explains 69.6% total variance ($r^2 = 0.60$; the given value is the cumulative percentage of the total pricipal component analysis (PCA) variance) in relation to

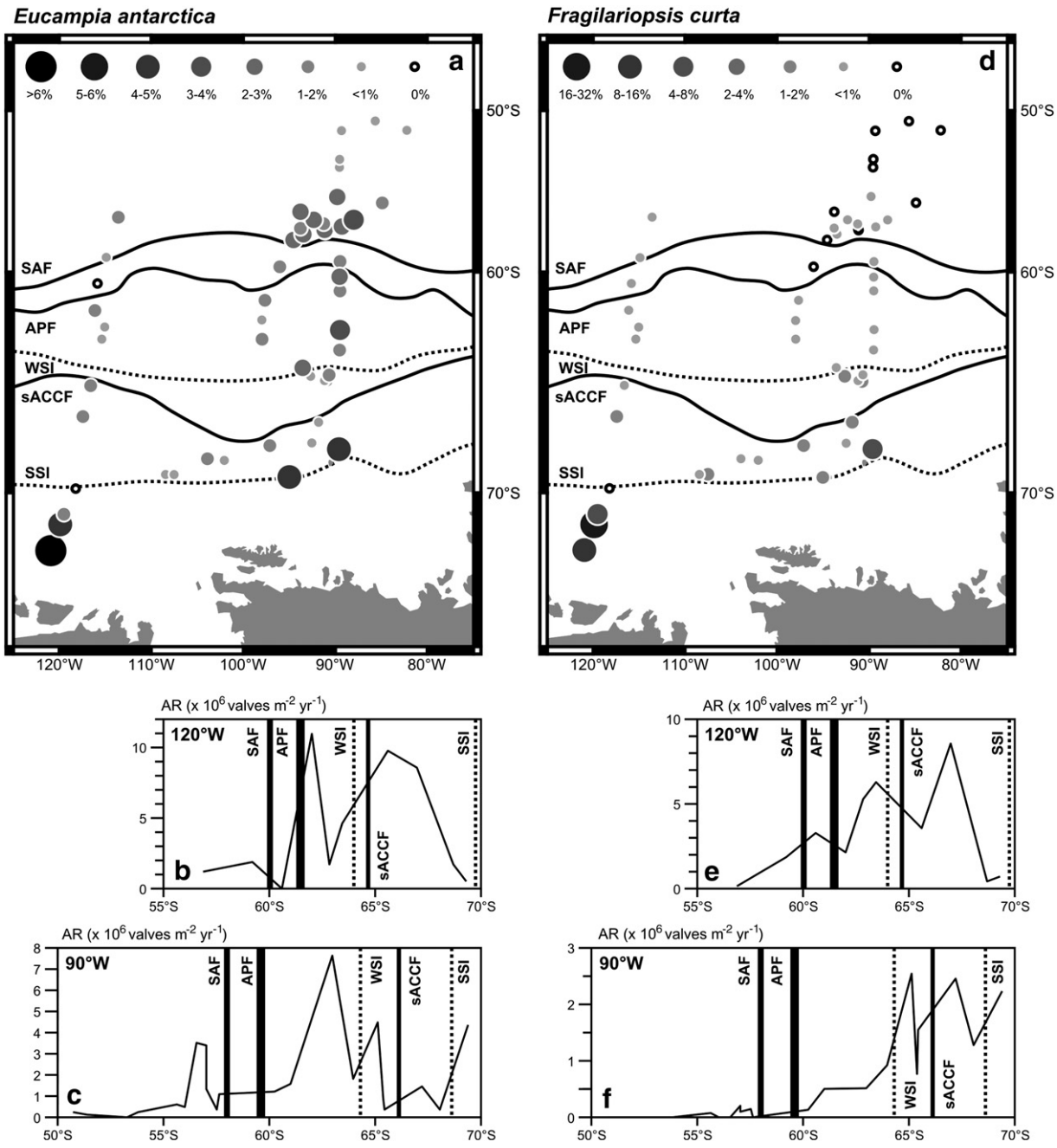

Fig. 8. Relative abundance maps and valve accumulation rates (AR) of the diatom species of the *Eucampia antarctica group* (a, b, c) and *Fragilariopsis curta* (d, e, f). Abbreviations as in Fig. 6.

the nine tested environmental variables, with 29.7% of variance explained by the first gradient and 15.6 % explained by the second gradient (Table 4). The remaining 30.4% of variance was unexplained by the nine tested variables and may be due to a variety of unexplored factors, but most likely the influence upon diatom preservation in the northern and southern zones of the study area compared to the central zone played an important role.

In the plot of sample distribution in relation to vectors reflecting the different environmental variables tested (Fig. 15a), the vectors of first order temperature (TEMP), salinity (SAL), and mixed layer depth (MLD) point in the direction of the lower left quadrant, whereas the vectors representing first order stratification (N) nitrate (NO_3) and phosphate (PO_4) point approximately in the opposite direction. The correlation of the environmental variables exhibits a certain amount of covariance among these six variables (Table 5), potentially biasing the results. The vectors reflect changing environmental conditions along the first canonical axis with decreasing temperature and salinity, and simultaneous increase of the dissolved nutrients NO_3, PO_4 and silicon (Si) (and sea ice concentration).

Fig. 15b identifies the samples located far north of the SAF with the highest negative values on the first canonical axis, and samples positioned near the SSIZ with the highest positive values on the first axis. Changes in value of the first RDA-axis follow a latitudinal gradient where high negative values were associated with low latitude sample stations (<−0.5) in conjunction with the SAF in the most eastern sector, and largest positive values (>0.5) corresponding to samples at the maximum average winter sea ice extent (Fig. 2h). Thus, the gradient of the first RDA-axis is assumed to reflect the relationship between species assemblages and one or more environmental variables (see Appendix B for the site scores of the polynomial RDA).

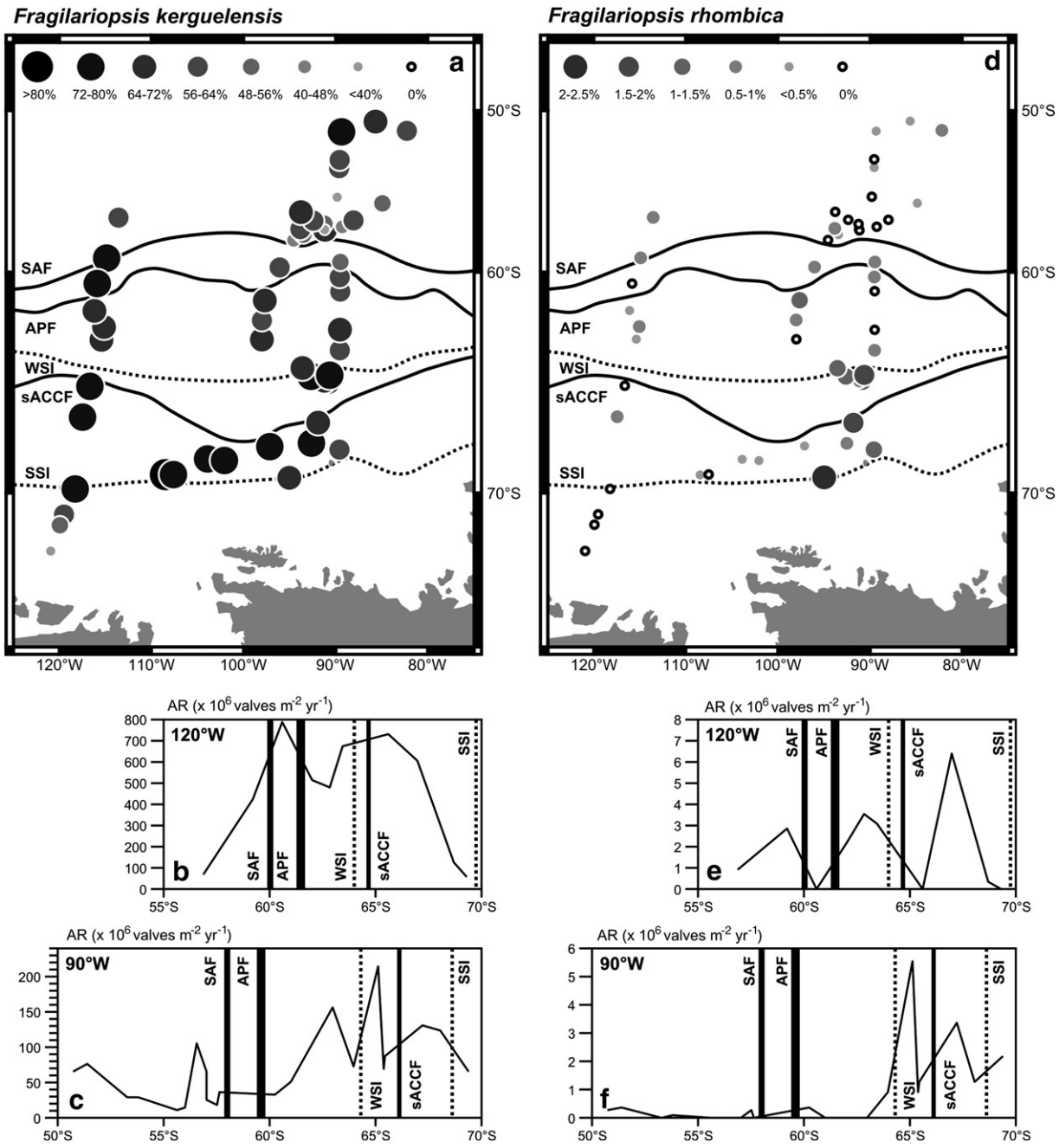

Fig. 9. Relative abundance maps and valve accumulation rates (AR) of the diatom species *Fragilariopsis kerguelensis* (a, b, c) and *Fragilariopsis rhombica* (d, e, f). Abbreviations as in Fig. 6.

A simple linear regression (only shown for temperature) between each variable and the first RDA-axis revealeds different coefficients of determination (r^2) for each variable (Table 6), with the strongest correlation observed with summer temperature ($r^2 = 0.941$; Fig. 15c), followed by annual nitrate ($r^2 = 0.908$), summer salinity ($r^2 = 0.819$) and annual phosphate ($r^2 = 0.791$) as secondary variance contributors. The remaining variables were less strongly associated to the first RDA-axis. For the second RDA-axis three variables could be significantly correlated ($r^2 > 0.2$; after Pearson's test of correlation coefficient significance) with the variance along this axis (Table 6): annual dissolved silicon (0.418) and mean winter and summer sea ice concentrations (0.264 and 0.646, respectively). This is in accordance with the geographical distribution of the sample locations: highest positive values on the second canonical axis are shown for the four stations annually affected by sea ice (Fig. 15a).

The polynomial RDA diagram for the relationship between species and the environmental variables (Fig. 16) indicated positive correlation or negative correlation between single species (for abbreviations see Table 2; see Appendix C for the species scores of the polynomial RDA) and vectors of environmental variables of first order (MLD, N, NO_3, PO_4, SAL, Si, SSIC, TEMP, and WSIC) and second order (MLD^2, N^2, NO_3^2, PO_4^2, SAL^2, Si^2, $SSIC^2$, $TEMP^2$, and $WSIC^2$). Generally, the environmental variable analysis shows strong covariance between TEMP, SAL, MLD, NO_3, PO_4 and N on one side and between Si, SSIC and WSIC on the other (Table 5). Focusing on the temperature/nutrient gradient, as the predominant factor in the site-related RDA (Fig. 15a), the species-related analysis reveals positive correlation only with *T. oestrupii* with first order TEMP, SAL and MLD, whereas *F. curta* and *F. cylindrus* show a negative correlation to these three variables. In contrast, *F. rhombica*, *F. ritscheri*, *F. separanda* and *T. gracilis* are

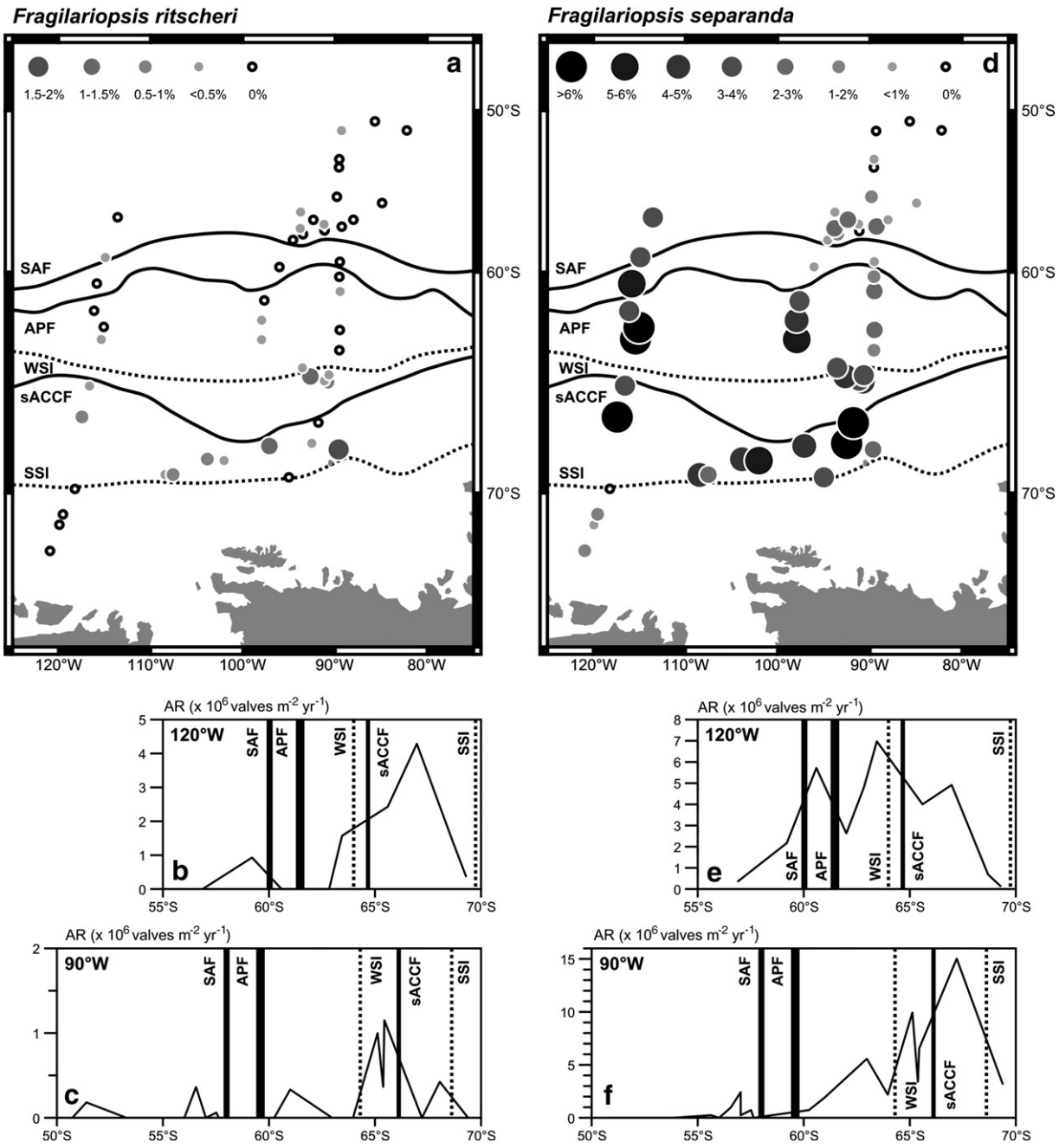

Fig. 10. Relative abundance maps and valve accumulation rates (AR) of the diatom species *Fragilariopsis ritscheri* (a, b, c) and *Fragilariopsis separanda* (d, e, f). Abbreviations as in Fig. 6.

negatively correlated to the second order TEMP^2. Species with no correlation to any of the environmental variables, either due to their very low relative abundance (e.g. *Fragilariopsis obliquecostata*; Fig. 4) or their equally high distribution across the whole temperature range (e.g. *F. kerguelensis*; Fig. 4) show very short or no vector length (Fig. 16). The vectors of *A. tabularis* var. *egregius*, *H. cuneiformis* and *R. tesselata* imply a relationship of the species abundance to the first and second order sea surface summer temperature and NO_3^2/PO_4^2 (Fig. 16). On the other hand, the variance in *F. curta* and *A. actinochilus,* and to a lesser degree *F. cylindrus* and *E. antarctica* group, are correlated either with changes in the mean annual dissolved silicon concentration of the upper water column or to the variance in winter and summer sea ice concentrations. However, the relationship between the diatom assemblage compositions and sea ice/dissolved silicon variation (second RDA-axis) is less distinct than the relationship with the temperature/nutrient variation (first RDA-axis) in explaining the main variance observed in the data set (Table 4).

5. Discussion

5.1. Diatom accumulation rates and opal deposition

The diatom valve concentration and ^{230}Th-normalised valve ARs, as well as BSi concentration (weight percent) and ^{230}Th-normalised BSi ARs display distinct differences between the eastern (90°W) and western (120°W) transects in terms of their magnitude and their latitudinal distribution pattern (Fig. 5). The magnitude of BSi deposition and the maximum deposition of BSi in a region between the SAF and the northern SSIZ observed along the western transect are similar to the values and the distribution pattern of BSi described by

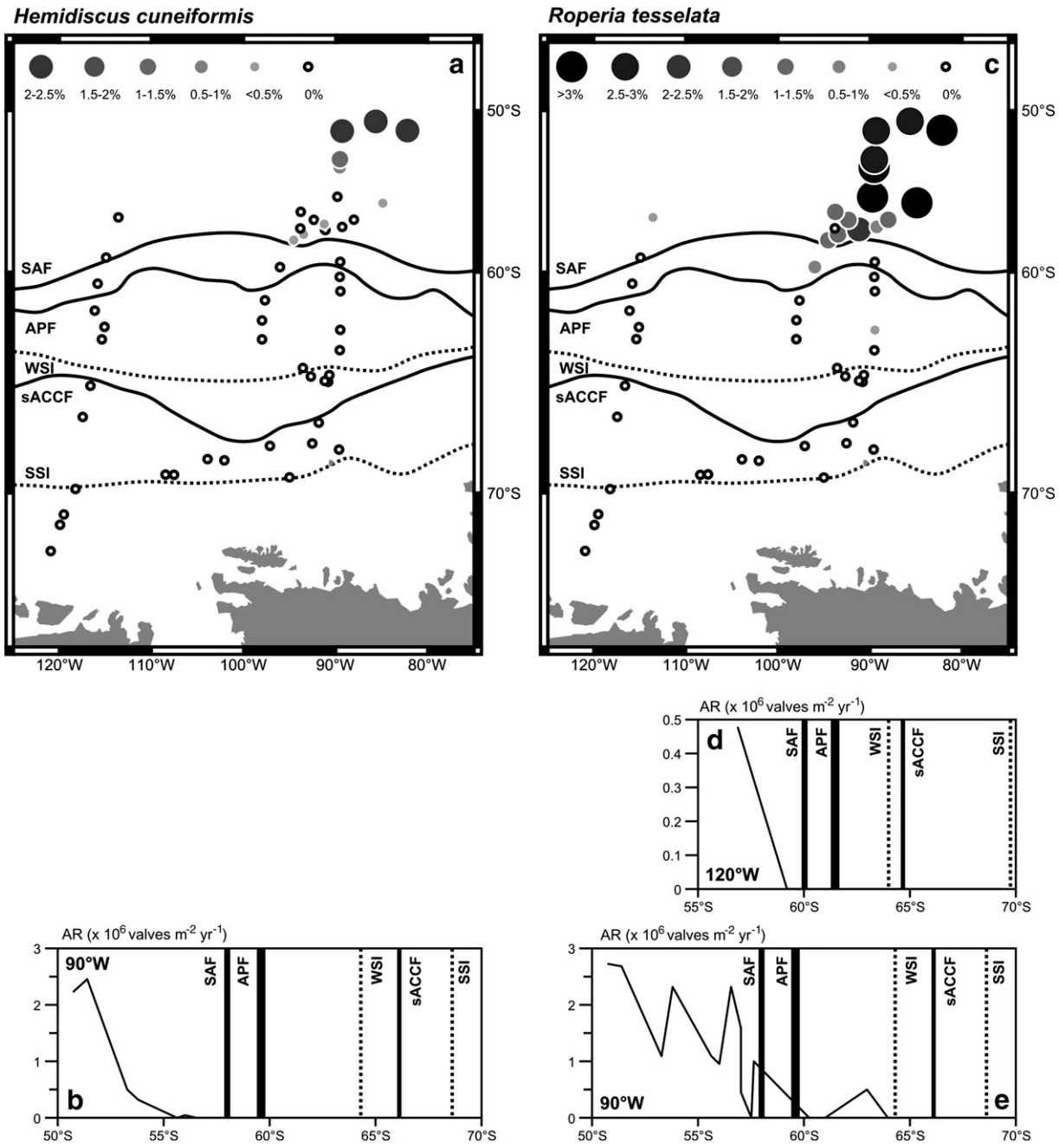

Fig. 11. Relative abundance maps and valve accumulation rates (AR) of the diatom species *Hemidiscus cuneiformis* (a, b) and *Roperia tesselata* (c, d, e). Abbreviations as in Fig. 6.

Geibert et al. (2005) from the Atlantic sector of the Southern Ocean. Similarly, our results match ^{230}Th-normalised BSI observations determined from the western Pacific sector around 170°W (Sayles et al., 2001) and the Indian sector along 110°E (François et al., 1997), where a zone of high BSi deposition spans between 800 and 1000 km in latitude. However, BSi ARs from the western Pacific, the Indian and Atlantic sectors may exceed the values at our 120°W transect by factors of 2 to 5 (DeMaster, 2002). Because diatom valve accumulation rates in this paper are the first to be presented from the Southern Ocean, comparisons concerning the contribution of diatom species to the deposited BSi in other sectors of the Southern Ocean can only be based on estimates of averaged BSi AR values and diatom species abundances from the same area. Diatom species distributions in surface sediments presented from the Atlantic and the Indian sectors (Zielinski and Gersonde, 1997; Crosta et al., 2005) indicate that *F. kerguelensis* represents the dominant species of the Southern Ocean open-ocean opal deposition, as documented by this study of the 120°W transect. Distinctly lower diatom valve and BSi deposition encountered along the 90°W transect (Fig. 5b,f) mark a sector of reduced biogenic opal deposition in the eastern South Pacific, which extends into the area of the Drake Passage (Geibert et al. 2005). Such reduction in BSi accumulation has already been remarked by DeMaster (1981). A distinct reduction of the Southern Ocean opal belt between 120°W and the Drake Passage has also been predicted by an annually averaged version of the Hamburg Ocean Carbon Cycle model (Ragueneau et al., 2000). The presence of this Southern Ocean "diatom deposition gap" requires explanation. Generally, macronutrient concentrations decline from west to east in the study area (Fig. 2), which may be related to the channelling effect of the Drake Passage. However, according to Holm-Hansen et al. (2005) this pattern should not have a distinct effect on biological productivity. They report overall low productivity between 140°W and 70°W (see

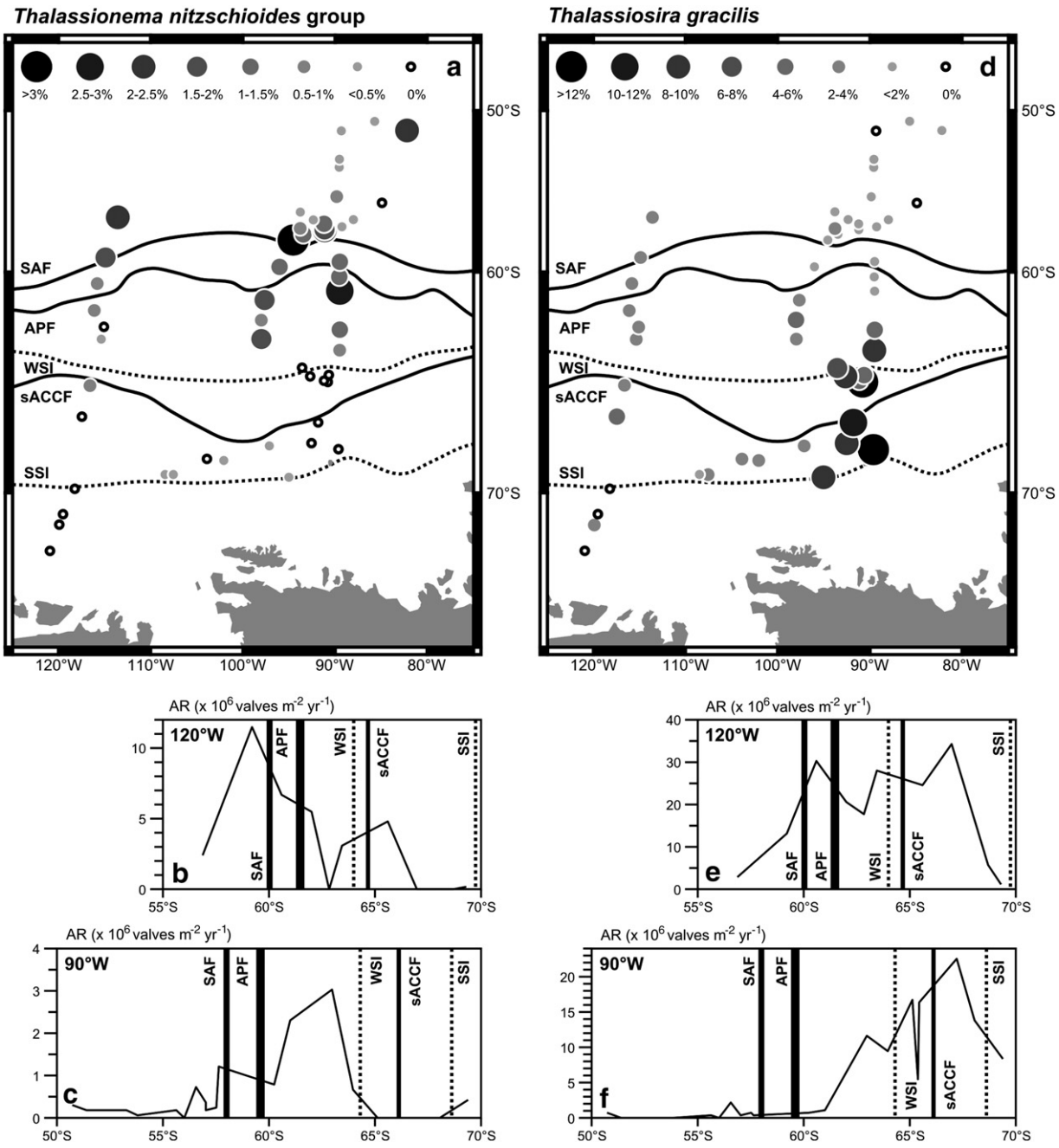

Fig. 12. Relative abundance maps and valve accumulation rates (AR) of the diatoms species groups *Thalassionema nitzschioides* group (a, b, c) and *Thalassiosira gracilis* (d, e, f). Abbreviations: APF: Antarctic Polar Front; sACCF: southern ACC Front; SAF: Subantarctic Front; SSI: maximum average summer sea ice extent; WSI: maximum average winter sea ice extent.

also Moore and Abbott, 2000), as a result of continental source trace element availability in this area. As such, it is unlikely that differences in diatom production are responsible for the uneven deposition of diatoms in the eastern and western sector of the study area and it follows that other factors must be considered to explain the observed decoupling of primary production from the distribution of diatom valve abundances and BSi preservation.

The discovery that bulk vertical sediment fluxes at both transects are of similar magnitude (Table 1), which results from higher terrigenous flux rates along the eastern transect (Geibert et al., 2005), helps to explain the inter-basin difference. Such a pattern is not supportive of an east-west differentiation of BSi deposition rates arising from generally lower sedimentation rates at 90°W, as a result of increased bottom water winnowing in the vicinity of the Drake Passage. However, increased deposition of terrigenous components in the deep basin of the Bellingshausen Sea may have an effect on the preservation of biogenic opal after its deposition at the sea floor. Increasing sediment ratios of terrigenous to BSi content has been reported as leading to a decrease in silicic acid concentration in pore waters and a reduction of BSi preservation (Ragueneau et al., 2000). Indeed, the sedimentary environments in the areas of the eastern and western transects are distinct. While the 90°W transect located across the flat Bellingshausen abyssal plain is supplied by distal turbidites from the tectonically active Antarctic Peninsula region (Nitsche et al., 2000; Robertson Maurice et al., 2003), along the 120°W transect deposition of terrigenous components by turbidites from the Antarctic margin is restricted by an undulated bottom topography, especially north of site PS58/265 (Fig. 1). Thus, we conclude the biogenic flux

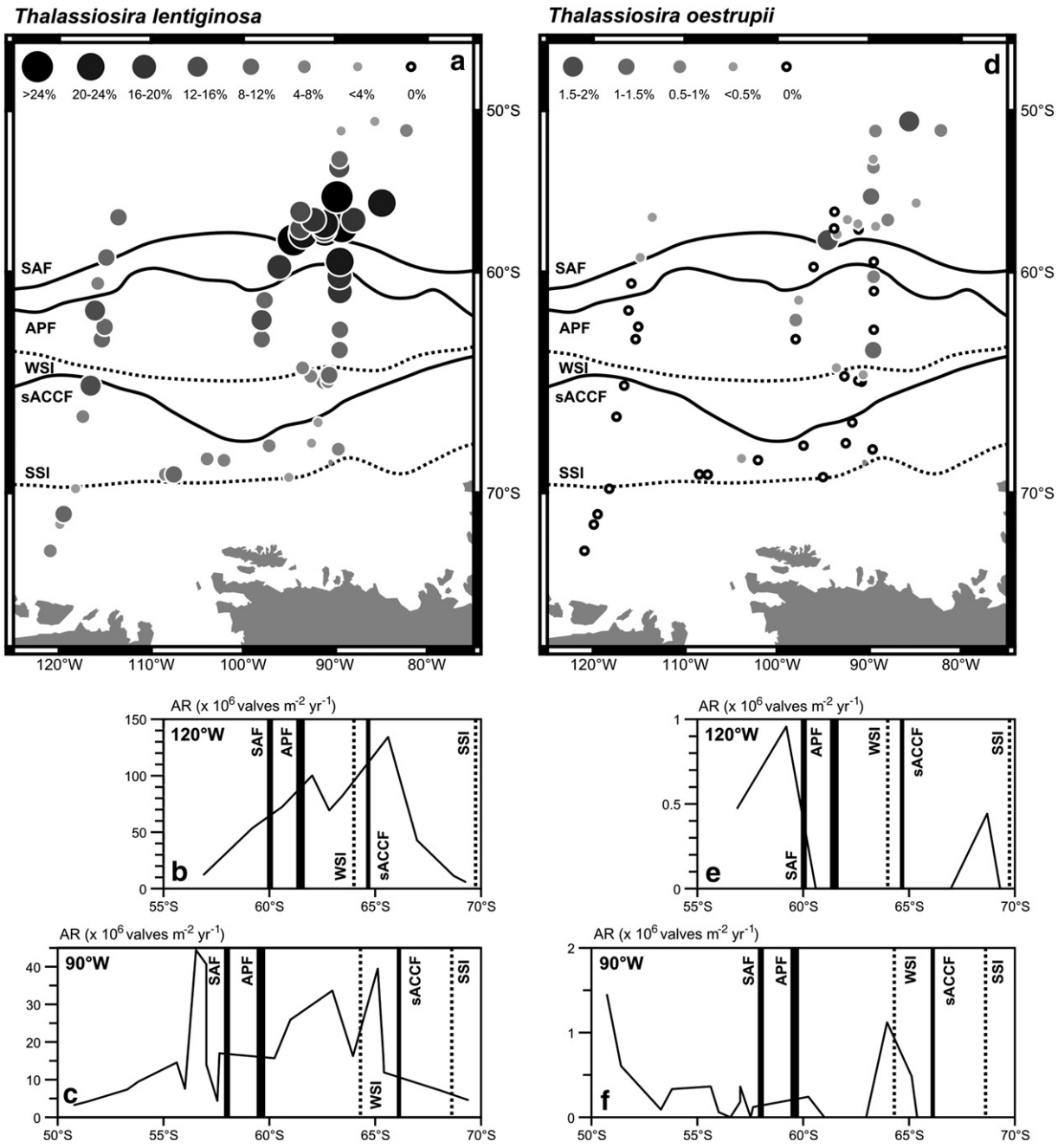

Fig. 13. Relative abundance maps and valve accumulation rates (AR) of the diatom species *Thalassiosira lentiginosa* (a, b, c) and *Thalassiosira oestrupii* (d, e, f). Abbreviations as in Fig. 6.

into the sediments is prone to higher dilution by terrigenous material along the eastern transect than in the western sector, accounting for the differantiation in diatom AR and BSi AR values presented here.

5.2. Diatom species distribution

The observed diatom distribution patterns are closely related to the oceanographic zones and the mean sea ice seasonal maxima in the study area and coincides well with the diatom distribution reported from other sectors of the Southern Ocean (Zielinski and Gersonde, 1997; Armand et al. 2005; Crosta et al., 2005; Romero et al., 2005). This pattern is not significantly disturbed, either by the east–west gradient in diatom accumulation and preservation or by the presence of large sediment drifts, debris flows and off-shore reaching channel systems at the Antarctic continental margin (Fig. 3). At the sites located near the continent, neither down-slope transport of neritic diatoms from the Antarctic shelf environment nor reworking of older fossil species could be detected.

5.2.1. Subantarctic Zone (SAZ)

Overlooking the elevated high abundances of species with large temperature ranges (e.g. *F. kerguelensis*, *T. lentiginosa*), the SAZ diatom assemblage was found to be characterised by typical warmer water dwellers, such as *A. tabularis* (both varieties), *H. cuneiformis*, *R. tesselata*, the *T. nitzschioides* group and *T. oestrupii*. This observation is in accordance with previous work carried out in the same area. Kozlova (1966) reported *F. kerguelensis* and *T. lentiginosa* to be dominant species in Subantarctic sediments of the Pacific sector. Considering that BSi and diatom valve preservation both decreased in the SAZ (Figs. 3 and 5), it can be assumed that the relative abundances of the heavily silicified *F. kerguelensis* and *T. lentiginosa* in this zone

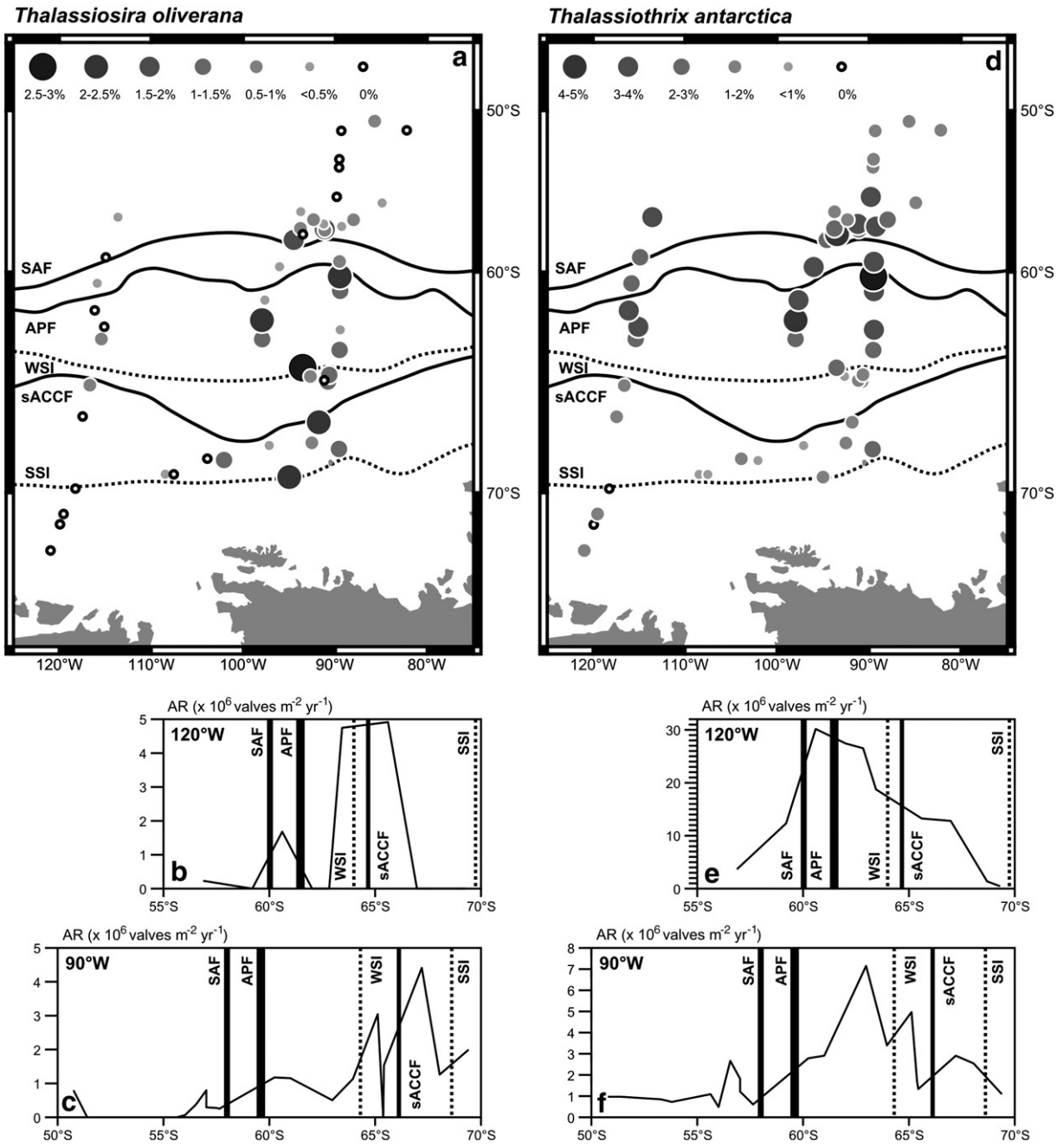

Fig. 14. Relative abundance maps and valve accumulation rates (AR) of the diatom species *Thalassiosira oliverana* (a, b, c) and *Thalassiothrix antarctica* (d, e, f). Abbreviations as in Fig. 6.

were enhanced as a result of their higher preservation efficiency (Burckle and Cirilli, 1987; Pichon et al., 1992a,b).

Remarkably, the variety *Azpeitia tabularis* var. *egregius* occurred in higher numbers only along the eastern transect north of the SAF (Fig. 6). This distribution pattern of *A. tabularis* var. *egregius* suggests a lower tolerance to colder temperatures compared to the variety *tabularis* (Fig. 4). This assumption is supported by the results of the polynomial RDA, showing the vector of *A. tabularis* var. *egregius* to point more in the direction of the environmental variable vectors TEMP and TEMP^2 then the vector of *A. tabularis* var. *tabularis* (Fig. 16). However, such a difference in the distribution pattern of both varieties has not been observed in other sectors of the Southern Ocean (e.g. Zielinski and Gersonde, 1997; Romero et al., 2005).

A census of diatom assemblages preserved in surface sediments from the Atlantic and Indian sectors of the Southern Ocean generally confirms our biogeographic distribution results obtained from the southeastern Pacific sector. *Roperia tesselata* and *H. cuneiformis* were exclusively encountered north of the SAF in the Atlantic and Indian sectors (Romero et al., 2005), with the exception of rare findings of *R. tesselata* in the Atlantic sector SAZ (Zielinski and Gersonde, 1997).

Table 4
Polynomial canonical redundancy analysis (RDA) results.

Polynomial RDA of 52 samples, 27 species/taxa, 9 environmental variables				
Axes	1	2	3	4
Canonical Eigenvalues	1.39	0.73	0.43	0.18
% of the total PCA variance	29.72	15.59	9.12	3.90
Cumulative % of the total PCA variance	29.72	45.31	54.43	58.33
Cumulative % of the canonical variance	42.69	65.08	78.18	83.78

PCA: Principal Component Analysis (the PCA is the first element of the polynomial RDA).

Other typical warm water dwellers, such as *Alveus*, *Fragilariopsis doliolus, Thalassionema nitzschioides* var. *parva* and *Rhizosolenia bergonii,* which have been encountered in the Atlantic and Indian sectors only north of the Subtropical Front or with a southernmost occurrence boundary in the northern SAF (Zielinski and Gersonde, 1997; Romero et al., 2005) have been found scattered and at very low numbers (<1% of assemblage), with exception to *A. marinus,* which was not detected in the set of samples studied (Table 2).

Significantly, a zone of increased occurrences of *Chaetoceros* spp. group and the *E. antarctica* group was observed along the 90°W transect in the southernmost SAZ close to the SAF. Although we did not distinguish between the two *E. antarctica* varieties reported by Fryxell and Prasad (1990), *E. antarctica* frustules observed in the SAZ might belong to *E. antactica* var. *recta*, whereas the increased occurrence of the *E. antarctica* group in the SSIZ (Fig. 8a) may be related to *E. antarctica* var. *antarctica*. Plankton studies confirm increased *Chaetoceros* and *E. antarctica* occurrences around 60°S in the study area (Hasle 1969; Fenner et al., 1976), but such distribution patterns have not been reported from previous surface sediment studies in the Atlantic and Indian sectors (Zielinski and Gersonde, 1997; Armand et al., 2005). de Baar et al. (2005) and Blain et al. (2007) have shown that both, *Chaetoceros spp.* and *Eucampia spp.,* were preferentially produced at nutrient conditions with elevated Fe-content. Dissolved Fe concentrations are generally very low in the eastern Southern Ocean Pacific because of its remoteness from upwind and upstream continental Fe source areas (e.g. Mahowald et al., 2005), but indeed a Fe-survey accomplished in the study area in late austral summer 1995 has found a slight Fe-enhancement in surface waters around 60°S in the PFZ (de Baar et al., 1999). Hints on the nature of the *Chaetoceros* resting spores can be derived from phytoplankton studies at 90°W reported by Hasle (1969). Her analysis of the *Brategg* samples results in a maximum (up to 0.4 10^6 cells l^{-1}) of *Chaetoceros neglectus* (belonging to the resting spore forming subgenus *Hyalochaetae*) around 60°S. Thus, the elevated numbers of *Chaetoceros* spp. spores

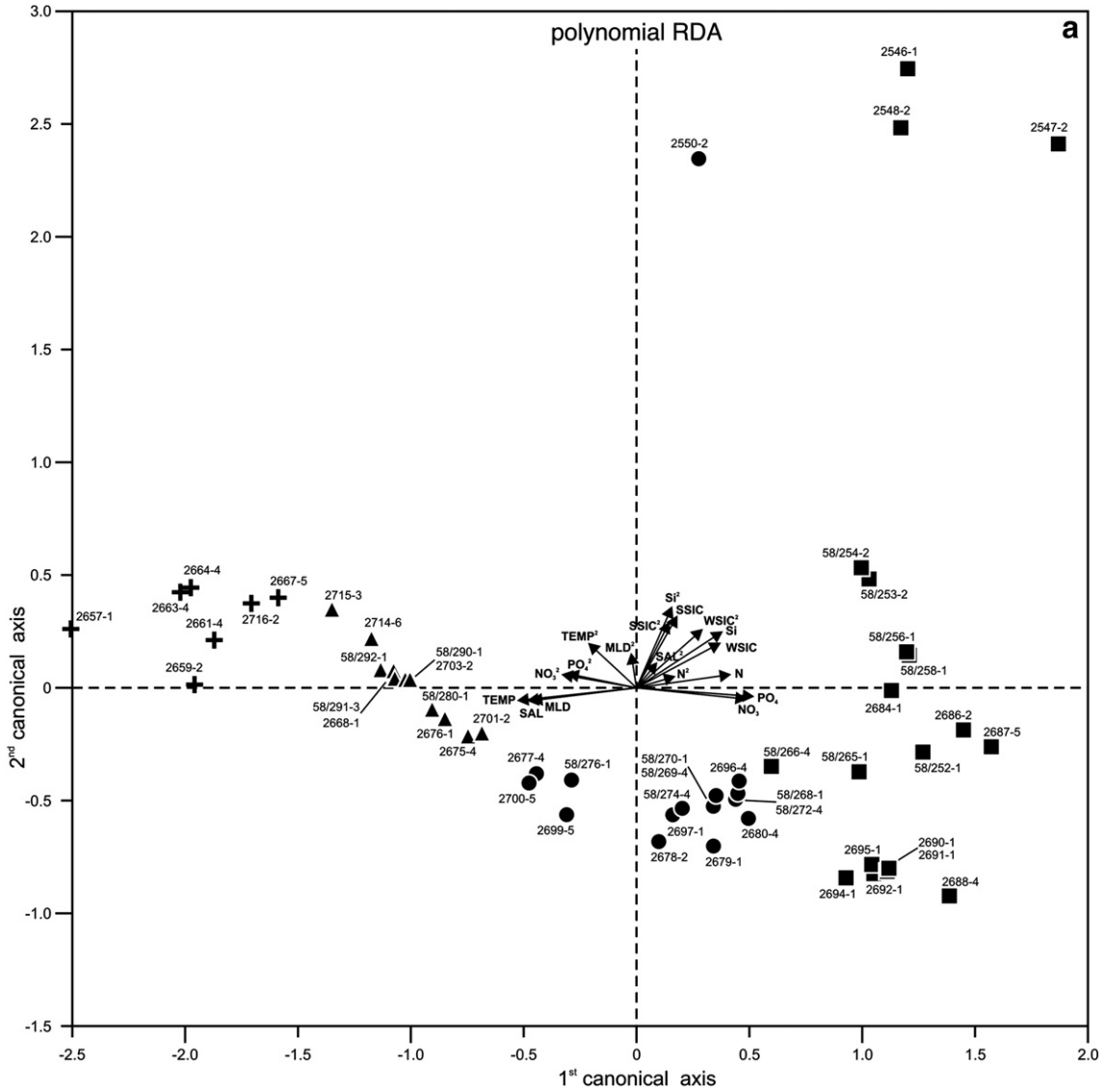

Fig. 15. a). Results of the polynomial Redundancy Analysis (RDA) showing variance in the diatom distribution (based on 26 selected species/species groups) in relation to the environmental variables of sea surface summer temperature (TEMP, $TEMP^2$) and salinity (SAL, SAL^2), mean annual surface water concentrations of dissolved nitrate (NO_3, NO_3^2), phosphate (PO_4, PO_4^2) and silicon (Si, Si^2), mean annual stratification of the water column (expressed in the Brunt–Väisälä frequency; N, N^2), the mean summer mixed layer depth (MLD, MLD^2) and mean winter and summer sea ice concentrations (WSIC, $WSIC^2$, SSIC, $SSIC^2$). b. Spatial distribution of the site score values of the polynomial RDA (crosses: < −1.5; triangles: −1.5 to −0.5; circles: −0.5 to 0.5; boxes: > 0.5). c. Regression plot of first axis polynomial RDA site scores versus sea surface summer temperature (SSST). The polynomial RDA accounts for 69.6% of total cummulative variance due to polynomial regression (mean coefficient of multiple determination = 0.60) and implies SSST to be the predominant environmental variable correlated with the diatom distribution ($r^2 = 0.941$).

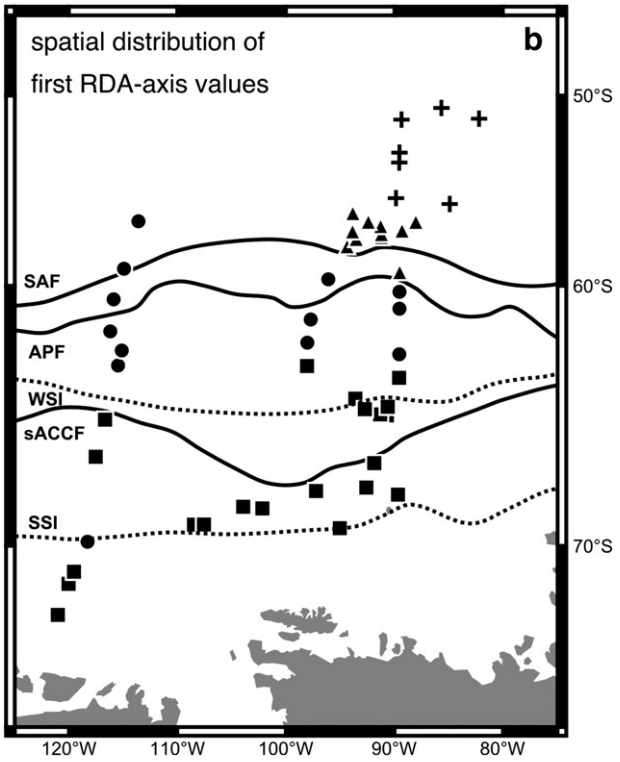

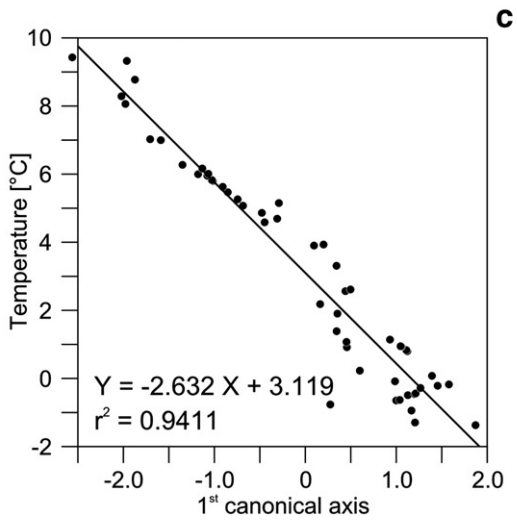

Fig. 15 (*continued*).

found in the SAZ of the studied region might reflect the increased production of *C. neglectus in this area.*

5.2.2. Polar Front Zone (PFZ) and Permanent Open Ocean Zone (POOZ)

As observed in the southern SAZ, *F. kerguelensis* represented one of the most prominent species of the PFZ and the POOZ of the southwest and central Pacific sector. The same finding was reported from the Indian and Atlantic sectors (Zielinski and Gersonde, 1997; Crosta et al., 2005). In spite of the eastward decrease in diatom preservation, the highest *F. kerguelensis* abundances were encountered the length of the 120°W transect. Along the 90°W transect the *F. kerguelensis* abundances were reduced by the occurrence of species such as *A. tabularis*, *T. gracilis* var. *gracilis* and *T. oliverana* (Figs. 6d, 7a,12d,14a). *Thalassiosira lentiginosa* represented the second most abundant species, especially in the SAZ and northern POOZ. Prominent occurrences of

Table 5
Correlation matrix of the 9 environmental variables.

	TEMP	SAL	NO_3	PO_4	Si	MLD	N	SSIC	WSIC
TEMP	1	0.927	−0.950	−0.911	−0.799	0.869	−0.801	−0.414	−0.754
SAL		1	−0.853	−0.834	−0.800	0.952	−0.919	−0.337	−0.836
NO_3			1	0.960	0.640	−0.822	0.718	0.243	0.582
PO_4				1	0.625	−0.821	0.684	0.188	0.546
Si					1	−0.792	0.744	0.739	0.905
MLD						1	−0.865	−0.364	−0.793
N							1	0.230	0.894
SSIC								1	0.575
WSIC									1

The grey bars highlight environmental variables covarying with others. The numbers indicate either strong positive or negative covariance if a threshold value of 0.8/−0.8 is exceeded.

this species (>15%) are related to a narrower and higher temperature range (4.5–6.5 °C) than *F. kerguelensis* (Figs. 9a and 13a). This pattern has not been reported from the Atlantic and Indian sectors, where both species have been related to a similar SSST range (Zielinski and Gersonde, 1997; Crosta et al., 2005). Other species encountered to occur widespreadly in the PFZ and the POOZ at significant abundances (>3%) and include *A. tabularis*, *F. separanda*, the *T. nitzschioides* group, *T. gracilis, T. oliverana* and *Thalassiothrix antarctica*.

Increased abundances of *F. separanda* (>3%) are associated with a SSST range between −0.5 and 4 °C and maximum abundances (>6%) occur between 0 and 1.5 °C, which is similar to the distribution range reported by Zielinski and Gersonde (1997) from the Atlantic sector. As such, the *F. separanda* distribution extends into the SSIZ, a pattern consistent with the compilation of *F. separanda* distribution data presented by Armand et al. (2005) from the Indian and Atlantic sectors (abundance >3% between −1 and 4 °C). Despite our study´s rather large distribution range extending from the SSIZ into the SAZ (Fig. 10d) and summaries of *F. separanda* having never been reported from any studies of sea ice samples (Zielinski and Gersonde, 1997; Armand et al., 2005), Armand et al. (2005) labelled *F. separanda* as one of the major sea ice related species, but also stated, that it had a "superficially poor relationship to sea ice parameters". They suggest that the wide temperature range results from lateral transport, but fail to explain why such transport mechanisms would only affect the distribution of *F. separanda* and not that of other sea ice related species. Also, the bottom water pathways in the SE Pacific sector, derived from pressure field differences (Fig. 3; Reid, 1986), and the flow pattern of freshly produced bottom water, identified by chlorofluorocarbon concentrations (Orsi et al., 1999; Rodehacke et al., 2007), show for the area south of 60°S a coastal-parallel bottom water flow in a westerly direction rather than a northward bottom layer transport. Thus, at least for the east Pacific sector, this makes lateral transport unlikely as an explanation for the higher abundances of *F. separanda* in sediments of the northern POOZ and north of the APF. Plankton studies in the Pacific sector (Hargraves, 1968) reported a broad distribution range of

Table 6
Correlation between the first and second RDA-axes and the 9 tested environmental variables.

Environmental variables	First RDA-axis[a]	Second RDA-axis[a]
TEMP	0.941	0.017
SAL	0.819	0.023
NO_3	0.908	0.010
PO_4	0.791	0.016
Si	0.505	0.418
MLD	0.748	0.026
N	0.611	0.028
SSIC	0.118	0.646
WSIC	0.491	0.264

[a] The values represent the coefficient of determination (r^2) for simple linar regressions between RDA-scores and environmental variables.

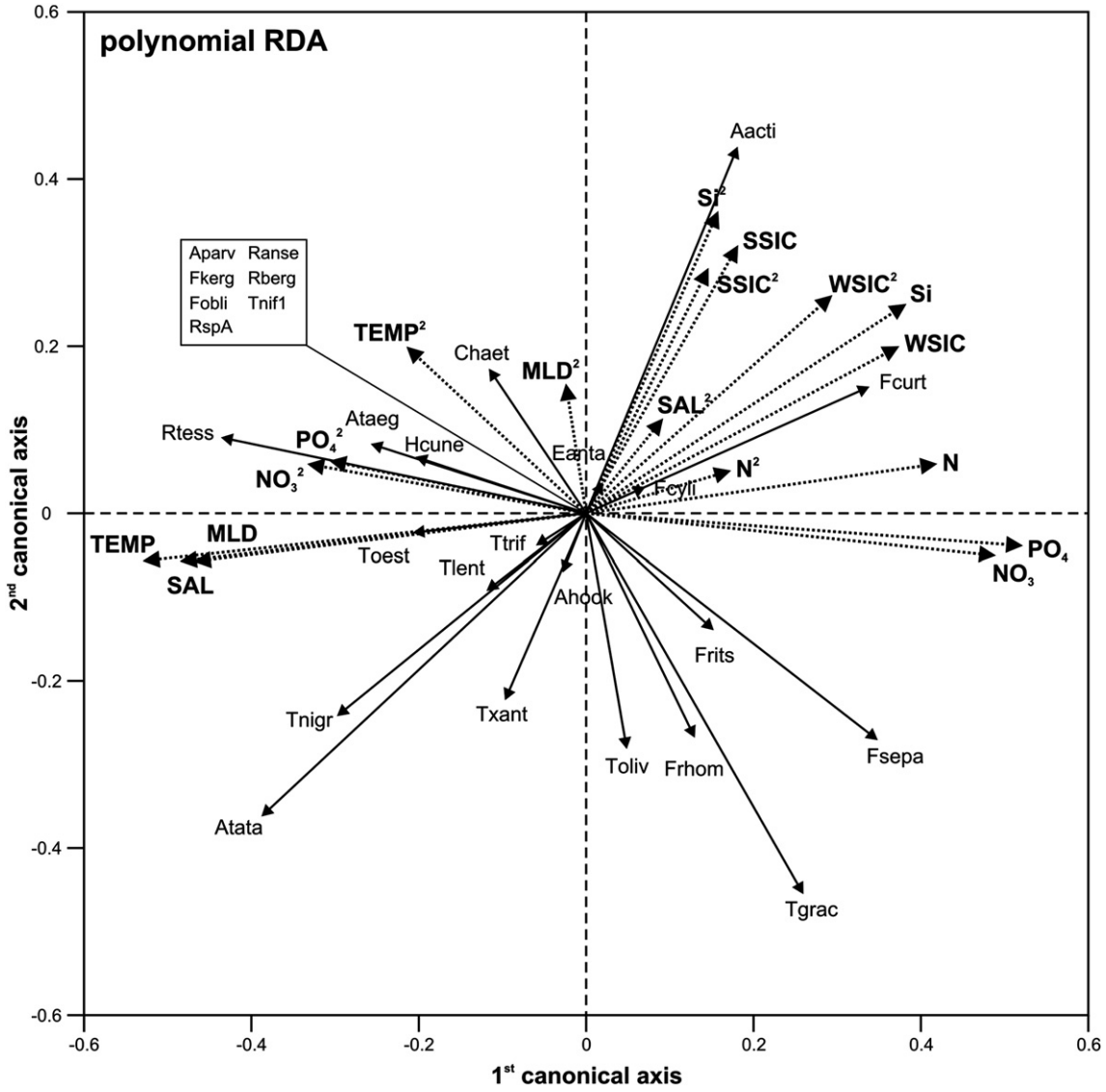

Fig. 16. Results of the polynomial RDA focused on the relationship between 26 diatom species/species groups (abbreviations are listed in Table 2) and the first and second order of environmental variables of mean summer sea surface temperature (TEMP, $TEMP^2$) and salinity (SAL, SAL^2), mean annual surface water concentrations of dissolved nitrate (NO_3, NO_3^2), phosphate (PO_4, PO_4^2) and silicon (Si, Si^2), mean annual stratification of the water column expressed in the Brunt–Väisälä frequency (N, N^2), the mean summer mixed layer depth (MLD, MLD^2) and mean winter and summer sea ice concentrations (WSIC, $WSIC^2$, SSIC, $SSIC^2$). The RDA plot shows a strong positive relationship between species and variables pointing in the same direction, and a strong negative relationship for species and variables pointing in the opposite direction, with the significance of the relationship given by the arrow length. No correlation between the variables and species are given for perpendicular plots of species (shown as inset box).

F. separanda in waters with temperatures between 1.2 and 8.7 °C, which makes it unlikely that *F. separanda* is a typical sea ice related taxon. The distribution of this species suggests a preference for surface waters free of sea ice at least during the summer season.

The abundance of the *T. nitzschioides* group decreased towards the south and dropped to values below 1% of the total diatom assemblage at SSSTs<3 °C. A similar pattern that has been reported from the Atlantic and Indian sectors (Zielinski and Gersonde, 1997; Crosta et al., 2005). In contrast, *Thalassiosira gracilis* abundances increased towards the SSIZ and reached maximum abundances in the SSIZ. This pattern relates *T. gracilis*>4% to SSSTs ranging between −1 and 3.5 °C, which is similar to the temperature relationship presented from the Atlantic and Indian sectors (Zielinski and Gersonde, 1997; Crosta et al., 2005), although Zielinski and Gersonde (1997) report occurrences >4% extending into waters with 6 °C during summer. *Thalassiothrix antarctica* displayed highest relative occurrences (5%) in the southeast Pacific POOZ, but has been encountered at values >1% in a broader zone extending from the SAF into the sea ice covered zone. Such a broad occurrence range was also gathered from the Atlantic and Indian sectors, reaching maximum values at a SSST range attributable to the northern POOZ and the PFZ (Zielinski and Gersonde, 1997; Crosta et al., 2005).

The general composition of the diatom assemblage observed in the POOZ and SSIZ characterises these two zones as areas of lower productivity and lower organic carbon export, compared to other sectors of the Southern Ocean. The overall dominance of *F. kerguelensis* valves on the sea floor is a significant indicator in this respect. Studies on the relationship between phytoplankton productivity and trace metal supply assumed that the lack of iron prevents the complete utilisation of ambient nitrate and influences phytoplankton species composition in open-ocean high nutrient low chlorophyll regimes (e.g. Hutchins and Bruland, 1998). Iron limitation increases the uptake of dissolved silicon, relative to nitrate and phosphorus. This led to the assumption that high grazing pressure on the regenerating microbial communities characteristic of the iron-limited Southern Ocean results in the accumulation of large, heavily silicified diatoms, such as *F. kerguelensis*, that drive the silicon pump (Smetacek et al., 2004). Consequently, higher biogenic opal accumulation in sedimentary records may reflect less productive surface water conditions

instead of high export production. The assumption of lower carbon export in the eastern Pacific sector compared to other Southern Ocean sectors is supported by the productivity studies of Arrigo et al. (1997, 1998) and may partially be a result of lower iron supply to the photic zone (de Baar et al., 1999).

5.2.3. Seasonal Sea Ice Zone (SSIZ) and Sea Ice Zone (SIZ)

The diatom assemblages in surface sediments of the southeastern Pacific sector SSIZ are characterised by *E. antarctica* group, *F. kerguelensis, F. ritscheri*, *F. separanda*, *F. rhombica* and *T. gracilis* var. *gracilis*. Prominent occurrence of these species has also been reported from the Atlantic and Indian SSIZ (Zielinski and Gersonde, 1997; Armand et al., 2005), but in contrast to these sectors, the occurrence of the "sea ice indicator" *F. curta* (Gersonde and Zielinski, 2000), which contributes up to >50% to the Atlantic and Indian SSIZ assemblages (Zielinski and Gersonde, 1997; Armand et al., 2005), was of minor importance (<2%) in the SSIZ of the south-eastern Pacific sector (Fig. 8d). The same observation was found to be true for *A. actinochilus* (Fig. 6a), a species that consistently co-occured with *F. curta* (reaching up to 4%) in the Atlantic and Indian SSIZ (Zielinski and Gersonde, 1997; Armand et al., 2005). This specific pattern may be related to the absence of stability-induced ice-edge blooms typically dominated by sea ice related diatom species reported from the Bellingshausen Sea SSIZ (Pollard et al., 1995; Savidge et al., 1995; Turner and Owens, 1995). The latter authors explained this bloom absence by the rapid southwards retreat of sea ice under the prevailing northerly winds in this region. Significantly, *F. kerguelensis* displays high abundances (up to 80%) in the east Pacific SSIZ at SSSTs between −0.5 and 2 °C (Fig. 9a). This differs from the data presented by Crosta et al. (2005) showing a distinct decrease in *F. kerguelensis* abundance at temperatures <1 °C. Zielinski and Gersonde (1997) also reported elevated *F. kerguelensis* abundances related to temperatures as low as −0.5 °C from the Weddell Sea embayment, but the *F. kerguelensis* abundance pattern in this region was considered strongly biased due to selective dissolution. Based on surface water studies, Hargraves (1968) reported a broad SSST range for *F. kerguelensis*, ranging from 10 °C in the SAZ to −1.6 °C in the pack ice environment of the SIZ. Furthermore, Hargraves (1968) correlated *F. curta* and *F. cylindrus* occurrences in the water column with the presence of pack ice and assumed these species to reflect sea ice conditions during their growing season. For *F. rhombica* Hargraves (1968) suggested a strong relationship to the SSIZ with a SSST range between 7.3 and 0.8 °C.

The relatively lower abundances of *F. curta* in sediments of the southeastern Pacific sector SSIZ compared to the other Southern Ocean sectors (Zielinski and Gersonde, 1997; Armand et al., 2005) may be related to the specific sea ice and productivity conditions in this area. Arrigo and colleagues (1997, 1998) characterised the eastern Pacific sector as one of the least productive areas of the Southern Ocean indicative of the low annual sea ice dynamics and very narrow SSIZ. In the Bellingshausen and the Amundsen Seas the modern sea ice coverage is generally restricted to latitudes south of 65°S (Comiso, 2003). In contrast, the Weddell Sea in the Atlantic sector has been characterised as displaying the largest annual sea ice variation, encompasses a broad marginal sea ice zone (the sea ice extends out to 55–60°S in winter; Comiso, 2003) and produces large areas of new-year ice (Comiso, 2003). Combined these circumstances result in favourable conditions that produce high diatomabundances related to seasonal sea ice melt back.

In relation to sea ice related primary production rates, the Indian sector is placed between the high production Atlantic and the low production eastern Pacific sectors (Arrigo et al., 1997, 1998). Thus, the increased *F. curta* abundances along the eastern Pacific transect at 120°W appear to be restricted to the southern SIZ.

The few study sites in our survey located in or at the edge of the SIZ affected by both winter and summer sea ice cover (Fig. 2), revealed lowest diatom concentrations and moderate to moderate–poor preserved diatom assemblages. The assemblages were affected by dissolution, but prominent occurrences include the typical sea ice indicators *F. curta* (up to 18%), and *A. actinochilus* (up to 11%), as well as *E. antarctica* group (up to 12.5%) and *Chaetoceros* spp. (up to 7.5%). Other Antarctic cold water taxa reported in areas affected by sea ice (Zielinski and Gersonde, 1997; Armand et al. 2005), such as *F. cylindrus, F. obliquecostata, F. sublinearis,* and *Porosira glacialis* are restricted to low numbers in our study (<2%) and display a scattered distribution (Fig. 4).

Previous studies on Amundsen Sea shelf sediments (Kellogg and Kellogg, 1987) and Bellingshausen Sea coastal sediments (Crosta et al., 1997) yielded additional information from the coastal environments adjacent to our study area. Kellogg and Kellogg (1987) reported the diatom assemblages from the Amundsen shelf sediments to be dominated by sea ice related algae (e.g. *F. curta*). The same was true for the Ross Sea embayment (Burckle et al., 1987; Cunningham and Leventer, 1998). These latter studies reported high *F. kerguelensis* abundances in the SSIZ sediments decreasing just south of the maximum summer sea ice extent and coincident increases of *F. curta* abundances towards the Antarctica inshore of the SIZ. In the northern sector of the Ross Sea SIZ, elevated concentrations of *F. curta* in the water column were not mirrored in the sediment record due to enhanced opal dissolution (Burckle et al., 1987). In contrast, the southern SIZ, characterised by the ice-free Ross Sea polynya (Arrigo and van Dijken, 2003), exhibited high abundances of *F. curta* both in the upper water column and in surface sediments (Burckle et al., 1987). This is in accordance with observations undertaken from the Pine Island Bay polynya (Kellogg and Kellogg, 1987) and reflects increased productivity and opal export in coastal polynyas, as assumed by Smith and Gordon (1997). However, the shorter settling time of diatoms over the shelf due to shallower water depth may have led to better opal preservation, resulting as well in higher *F. curta* abundance in the sediments.

Diatom assemblages preserved in surface sediments gathered from nearshore sites off the Antarctic Peninsula as well as from the Bransfield Strait and from sediment trap experiments (Bransfield Strait) are dominated by *Chaetoceros* spp. (Gersonde and Wefer, 1987; Abelmann and Gersonde, 1991; Crosta et al., 1997; Zielinski and Gersonde, 1997). Increased *Chaetoceros* spp. values have also been found in the samples from the SIZ in the study area (Fig. 7d,e), but have been deposited at much lower rates compared with the deposition in the Antarctic Peninsula region. Fenner et al. (1976) reported *Chaetoceros* spp. abundances of 10–18% in the plankton from the eastern Amundsen Sea at about 69°S, 98°W. Considering that plankton studies in the nearshore environments of the Antarctic Peninsula show that most of the spore-forming *Chaetoceros* (*Hyalochaetae*) in this area are associated to *C. socialis* (von Bodungen, 1986; Bode et al., 2002; Garibotti et al., 2005) it is rather likely that the *Chaetoceros* spores encountered in the studied SIZ are related to this taxon, while the spores from the open-ocean Subantarctic sites are most probably related to *C. neglectus*. Garibotti et al. (2005) document overwhelming occurrences of *C. socialis* (0.2–3.2 10^6 cells l^{-1}) from austral summer blooms (1996, 1997, 1999) sampled nearshore west of the Antarctic Peninsula, while other *Hyalochaetae* (e.g. *C. neglectus*) play a very minor role.

5.3. Implications of the polynomial RDA

The application of the polynomial RDA on the relative abundances of 27 diatom species and species groups from 52 surface sediment samples revealed strong relationships between diatom species abundances and environmental gradients. Among the 9 tested environmental variables, the diatom assemblage distribution was influenced in the first order by sea surface summer temperature variability. Such a relationship between the spatial diatom distribution in surface sediments and SSSTs has been revealed in the Atlantic and Indian sectors of the Southern Ocean by use of the Q-mode factor

analysis (Crosta et al., 1998a; Zielinski et al, 1998). This confirms the assumption, that the strong relationship between SSST and diatom distribution occurs circum-Antarctic wide, allowing for the use of transfer-function-based palaeotemperature reconstructions in circum-polar regions with low or even no coverage with modern diatom reference data.

Besides the strong influence of the temperature gradient the polynomial RDA revealed a secondary influence on the diatom species distribution. Variation in the summer and winter sea ice concentrations as well as dissolved silicon could be related to the variance in diatom abundances. A strong relationship between sea ice coverage and diatom distribution in the Southern Ocean has previously been reported from other sectors of the Southern Ocean (e.g. Armand et al., 2005). Regional reference data sets have been used for a quantitative palaeo sea ice reconstruction from the Indian sector (Crosta et al., 1998a, 2004). However, these approaches on the base of the Modern Analogue Technique required reference samples in vicinity of the palaeo-record to be reconstructed. With the application of a statistical method based on polynomial RDA a transfer function may be created to reconstruct palaeo sea ice extent in regions with less information on modern diatom distribution. However, taking the different circum-Antarctic sea ice regimes into account, additional information from less studied regions, such as the western Pacific sector, have to be gained to confirm such a circum-Antarctic relationship between diatoms and sea ice.

6. Summary and conclusions

This study presents the first more comprehensive and quantitative documentation of the diatom distribution in surface sediments of the Pacific sector of the Southern Ocean. The studied diatom assemblages are from 52 sample sites mostly aligned on two latitudinal transects, one across the Bellingshausen Sea (at 90°W) and the other across the Amundsen Sea (at 120°W). The diatom valve accumulation rates obtained from the 120°W transect are generally one order of magnitude higher than those from the eastern transect, with highest values (8–10×10^8 valves $m^{-2}\,yr^{-1}$) between the SAF and the northern SSIZ, extending over ca. 900 km between 60°S and 68°S. The distinctly lower diatom valve and BSi deposition encountered at the 90°W transect marks a sector of reduced biogenic opal deposition in the southeastern Pacific, which extends into the area of the Drake Passage.

The major diatom contributor to the BSi preserved at the sea floor is the heavily silicified *F. kerguelensis*. This species alone contributes >50% to the diatom assemblages in 47 out of the 52 examined sites. Its species AR pattern emulates the patterns of total diatom valve AR and the BSi AR. The rather large and strongly silicified valves of *T. lentiginosa* represented another prominent contributor to the total amount of diatom valve AR and BSi AR. Although dissolution affected the diatom assemblages from SAZ, southern SSIZ and SIZ sediments as a result of low diatom productivity and BSi export to the sea floor, the observed diatom species distribution patterns were distinctly related to the oceanographic zones and the seasonal sea ice maxima in the study area. With some exceptions, the observed distribution pattern coincides well with the diatom distribution reported from other sectors of the Southern Ocean. The significance of our results aids in confirming the circumpolar distribution of diatom species remains around the Southern Ocean.

SAZ diatom assemblages were characterised by typical warmer water dwellers such as *A. tabularis* (both varieties), *H. cuneiformis*, *R. tesselata*, *T. nitzschioides* group and *T. oestrupii*. *Chaetoceros* spp., probably belonging to *C. neglectus*, were found to increase close to the SAF. This increase in *Chaetoceros* spp. abundance is accompanied by prominent occurrences of *F. kerguelensis* and *T. lentiginosa*. Species encountered commonly in the PFZ and the POOZ at abundances >3% include *A. tabularis*, *F. separanda*, *F. kerguelensis*, the *T. nitzschioides* group., the *T. gracilis* group, *T. lentiginosa, T. oliverana* and *Thalassiothrix antarctica*. In surface sediments of the SSIZ the diatom assemblages are characterised by the *E. antarctica* group, *F. kerguelensis, F. ritscheri*, *F. separanda*, *F. rhombica* and the *T. gracilis* group. Although this zone is affected by winter sea ice, typical sea ice related species (*A. actinochilus, F. curta*) displayed only minor occurrences. The study sites located in or at the edge of the SIZ generally contained the lowest diatom concentrations and moderate to moderate–poor preserved diatom assemblages, distinct from the assemblages in the frontal zones north of the SIZ including typical sea ice related species (*A. actinochilus, F. curta*) , but also *Chaetoceros* spp. (probably related to *C. socialis*) and *E. antarctica* (E. antarctica var. recta most likely).

The polynomial canonical redundancy analysis of the relative diatom abundances explains 69.6% total variance in relation to the 9 tested environmental variables (Table 3), with 29.7% of variance explained by the first gradient and 15.6% explained by the second gradient. The polynomial RDA suggests that diatom assemblage compositions and distribution are mainly related to the variance in summer sea surface temperatures and to a lesser degree to the variance of mean summer sea ice concentration, dissolved silicon and mean winter sea ice concentration.

The new data set presented here represents a significant extension of the existing diatom surface sediment data sets from the Southern Ocean so far used for quantitative palaeoceanographic and palaeoenvironmental studies. However, a further extension into the western sector of the Southern Ocean Pacific is needed. Considering the results presented by Cassar et al. (2007), the composition and abundance pattern of western Pacific diatom assemblages may be affected by increased Fe-influx from Australia and New Zealand.

Acknowledgements

The authors are grateful to the anonymous reviewers for constructive reviews and comments on the manuscript. We thank R. Crawford, G. Cortese and C.L. De La Rocha for useful comments and a fruitful discussion. We acknowledge the technical assistance of U. Bock and R. Cordelair. This study was supported by grants from the German Israel Foundation (GIF) and the DFG-Research Center/Cluster of Excellence “The Ocean in the Earth System" in Bremen, Germany.

Appendix A. Taxonomy

SUBCLASS – *ORDER* – Family – *Genus* – *species*

Class: BACILLARIOPHYCEAE

BACILLARIOPHYCIDAE

BACILLARIALES

Bacillariaceae

Fragilariopsis Hustedt in Schmidt 1913
F. curta (Van Heurck) Hustedt 1958
F. cylindrus (Grunow) Krieger in Helmcke and Krieger 1954
F. doliolus (Wallich) Medlin and Sims 1993
F. kerguelensis (O´Meara) Hustedt 1952
F. obliquecostata (Van Heurck) Heiden in Heiden and Kolbe 1928
F. rhombica (O´Meara) Hustedt 1952
F. ritscheri Hustedt 1958
F. separanda Hustedt 1958
F. sublinearis (Van Heurck) Heiden in Heiden and Kolbe 1928
Nitzschia Hassal 1845
N. bicapitata Cleve 1901
N. kolaczeckii Grunow 1867
Pseudo-nitzschia Peragallo in Peragallo and Peragallo 1900
P. turgiduloides (Hasle) Hasle 1993

Class: COSCINODISCOPHYCEAE
BIDDULPHIOPHYCIDAE
BIDDULPHIALES
Biddulphiaceae
Eucampia Ehrenberg 1839
E. antarctica (Castracane) Mangin 1915
CHAETOCEROTOPHYCIDAE
CHAETOCEROTALES
Chaetocerotaceae
Chaetoceros Ehrenberg 1844
Chaetoceros spp
COSCINODISCOPHYCIDAE
ASTEROLAMPRALES
Asterolampraceae
Asteromphalus Ehrenberg 1844
A. hookeri Ehrenberg 1844
A. hyalinus Karsten 1905
A. parvulus Karsten 1905
COSCINODISCALES
Hemidiscaceae
Actinocyclus Ehrenberg 1837
A. actinochilus (Ehrenberg) Simonsen 1982
A. curvatulus Janisch in A. Schmidt et al. 1874–1959
Azpeitia M. Peragallo in Tempére and Peragallo 1912
A. tabularis var. egregius (Rattray) Hustedt 1930
A. tabularis var. *tabularis* (Grunow) Fryxell and Sims in Fryxell et al. 1986
Hemidiscus Wallich 1860
H. cuneiformis Wallich 1860
Roperia Grunow ex Pelletan 1889
R. tesselata (Roper) Grunow ex Pelletan 1889
RHIZOSOLENIOPHYCIDAE
RHIZOSOLENIALES
Rhizosoleniaceae
Rhizosolenia Brightwell 1858
R. species A Armand and Zielinski 2001
R. antennata (Ehrenberg) Brown 1920 forma *antennata*
R. antennata (Ehrenberg) Brown 1920 forma *semispina* Sundström 1986
R. bergonii H. Peragallo 1892
THALASSIOSIROPHYCIDAE
THALASSIOSIRALES
Thalassiosiraceae
Porosira Jørgensen 1905
P. glacialis (Grunow) Jørgensen 1905
Thalassiosira Cleve 1873
T. antarctica Comber 1896
T. frenguelliopsis Fryxell and Johansen 1985
T. gracilis (Karsten) Hustedt 1958
T. gravida Cleve 1896
T. lentiginosa (Janisch) Fryxell 1977
T. oestrupii (Ostenfeld) Hasle 1972
T. oliverana (O´Meara) Makarova and Nikolajev 1983
T. trifulta Fryxell in Fryxell and Hasle 1979
T. tumida (Janisch) Hasle in Hasle et al. 1971
Class: FRAGILARIOPHYCEAE
FRAGILARIOPHYCIDAE
THALASSIONEMATALES
Thalassionemataceae
Thalassionema Peragallo 1908–1910
T. nitzschioides forma 1 Zielinski and Gersonde 1997
T. nitzschioides var. *capitulata* (Castracane) Moreno-Ruiz and Licea 1995
T. nitzschioides var. *lanceolata* (Grunow) Peragallo and Peragallo 1897
T. nitzschioides var. *parva* (Heiden) Moreno-Ruiz and Licea 1995
Thalassiothrix Cleve and Grunow 1880
T. antarctica Schimper ex Karsten 1905

Appendix B. Site scores of the polynomial RDA

Site	1st axis	2nd axis	Site	1st axis	2nd axis
PS 2546-1	1.323	2.626	PS 2696-4	0.374	−0.632
PS 2547-2	2.026	2.478	PS 2697-1	−0.160	−0.447
PS 2548-2	1.010	2.282	PS 2699-5	−0.038	−0.525
PS 2550-2	0.324	2.871	PS 2700-5	−0.289	−0.741
PS 2657-1	−2.654	0.354	PS 2701-2	−0.151	−0.520
PS 2659-2	−1.760	0.010	PS 2703-2	−1.765	0.086
PS 2661-4	−1.794	0.743	PS 2714-6	−0.648	0.203
PS 2663-4	−1.869	0.380	PS 2715-3	−0.892	0.033
PS 2664-4	−2.253	0.744	PS 2716-2	−1.430	0.555
PS 2667-5	−1.668	0.314	PS 58/252-1	1.354	−0.226
PS 2668-1	−0.977	−0.148	PS 58/253-2	0.889	0.654
PS 2675-4	−1.059	−0.258	PS 58/254-2	0.932	0.347
PS 2676-1	−1.711	−0.340	PS 58/256-1	1.326	0.614
PS 2677-4	−1.046	−0.168	PS 58/258-1	0.943	0.076
PS 2678-2	−0.079	−0.891	PS 58/265-1	1.109	−0.379
PS 2679-1	0.189	−1.079	PS 58/266-4	0.548	−0.420
PS 2680-4	0.592	−0.577	PS 58/268-1	0.676	−0.638
PS 2684-1	1.403	−0.398	PS 58/269-4	0.673	−0.192
PS 2686-2	1.784	−0.191	PS 58/270-1	0.158	−0.374
PS 2687-5	1.490	−0.404	PS 58/272-4	0.198	−0.323
PS 2688-4	1.225	−0.763	PS 58/274-4	−0.039	−0.502
PS 2690-1	1.568	−1.244	PS 58/276-1	−0.642	−0.693
PS 2691-1	1.164	−0.414	PS 58/280-1	0.374	−0.519
PS 2692-1	1.061	−0.611	PS 58/290-1	−1.871	0.063
PS 2694-1	0.842	−0.803	PS 58/291-3	−1.087	0.506
PS 2695-1	1.500	-0.678	PS 58/292-1	−1.172	0.157

Appendix C. Species scores of the polynomial RDA (normalised eigenvectors)

Species or species group	Abbrev.	1st axis	2nd axis
Actinocyclus actinochilus	Aacti	0.180	0.439
Asteromphalus hookeri	Ahook	−0.026	−0.070
Asteromphalus parvulus	Aparv	0.023	0.022
Azpeitia tabularis var. egregius	Ataeg	−0.257	0.085
Azpeitia tabularis var. *tabularis*	Atata	−0.388	−0.361
Chaetoceros spp.	Chaet	−0.114	0.176
Eucampia antarctica group	Eanta	0.022	0.039
Fragilariopsis curta	Fcurt	0.341	0.154
Fragilariopsis cylindrus	Fcyli	0.071	0.033
Fragilariopsis kerguelensis	Fkerg	0.027	−0.022
Fragilariopsis obliquecostata	Fobli	0.024	−0.014
Fragilariopsis rhombica	Frhom	0.130	−0.266
Fragilariopsis ritscheri	Frits	0.152	−0.136
Fragilariopsis separanda	Fsepa	0.332	−0.278
Hemidiscus cuneiformis	Hcune	−0.204	0.069
Rhizosolenia antennata f. *antennata*	Ranse	−0.024	−0.033
Rhizosolenia bergonii	Rberg	−0.030	−0.014
Rhizosolenia species A	RspA	−0.002	−0.029
Roperia tesselata	Rtess	−0.436	0.093
Thalassionema nitzschioides f. 1	Tnif1	−0.017	−0.003
Thalassionema nitzschioides group	Tnigr	−0.296	−0.241
Thalassiosira gracilis group	Tgrac	0.267	−0.479
Thalassiosira lentiginosa	Tlent	−0.117	−0.091
Thalassiosira oestrupii	Toest	−0.207	−0.022
Thalassiosira oliverana	Toliv	0.050	−0.280
Thalassiosira trifulta	Ttrif	−0.054	−0.028
Thalassiothrix antarctica	Txant	−0.095	−0.221

References

Abelmann, A., Gersonde, R., 1991. Biosiliceous particle flux in the Southern Ocean. Mar. Chemistry 35, 503–536.

Abelmann, A., Gersonde, R., Cortese, G., Kuhn, G., Smetacek, V., 2006. Extensive phytoplankton blooms in the Atlantic sector of the glacial Southern Ocean. Paleoceanogr. 21, PA1013. doi:10.1029/2005PA001199.

Armand, L.K., Leventer, A., 2003. Palaeo sea ice distribution; its reconstruction and significance. In: Thomas, D.N., Dieckmann, G.S. (Eds.), Sea ice: an Introduction to its Physics, Biology, Chemistry, and Geology. Blackwell Science, Oxford, pp. 333–372.

Pichon, J.J., Labeyrie, L.D., Bareille, G., Labracherie, M., Duprat, J., Jouzel, J., 1992a. Surface water temperature changes in the high latitudes of the Southern Hemisphere over the last Glacial–Interglacial cycle. Paleoceanogr. 7 (3), 289–318.

Armand, L.K., Leventer, A., 2009. Palaeo sea ice distribution and reconstruction derived from the geological records, In: Thomas, D.N., Dieckmann, G.S. (Eds.), Sea Ice, 2nd ed. Wiley-Blackwell. 640 pp.

DeMaster, D.J., 1981. The supply and removal of silica from the marine environment. Geochim. Cosmochim. Acta 45, 1715–1732.

Armand, L.K., Zielinski, U., 2001. Diatom species of the genus *Rhizosolenia* from Southern Ocean sediments: distribution and taxonomic notes. Diatom Res. 16 (2), 259–294.

Armand, L.K., Crosta, X., Romero, O., Pichon, J.-J., 2005. The biogeography of major diatom taxa in Southern Ocean sediments: 1. Sea ice related species. Palaeogeogr., Palaeoclimatol. Palaeoecol. 223, 93–126.

Arrigo, K.R., van Dijken, G.L., 2003. Phytoplankton dynamics within 37 Antarctic coastal polynya systems. J. Geophys. Res. 16 (C8), 3271. doi:10.1029/2002JC001739.

Arrigo, K.R., Worthen, D.L., Lizotte, M.P., Dixon, P., Dieckmann, G., 1997. Primary production in Antarctic Sea Ice. Science 276, 394–397.

Arrigo, K.R., Worthen, D., Schnell, A., Lizotte, M.P., 1998. Primary production in Southern Ocean waters. J. Geophys. Res. 103 (C8), 15 587–15 600.

Baker, A.D.C., 1954. The circumpolar continuity of Antarctic plankton species. Discovery Reports XXVIII, 2001–2218.

Bianchi, C., Gersonde, R., 2002. The Southern Ocean surface between marine isotope stages 6 and 5d: shape and timing of climate changes. Palaeogeogr., Palaeoclimatol. Palaeoecol. 187, 151–177.

Bianchi, C., Gersonde, R., 2004. Climate evolution at the last deglaciation: the role of the Southern Ocean. Earth Planet. Sci. Letters 228, 407–424.

Birks, H.J.B., 1998. Numerical tools in palaeolimnology — progress, potentialities, and problems. J. Palaeolimnol. 20, 307–332.

Blain, S., Quéguiner, B., Armand, L., Belviso, S., Bombled, B., Bopp, L., Bowie, A., Brunet, C., Brussaard, C., Carlotti, F., Christaki, U., Corbiére, A., Durand, I., Ebersbach, F., Fuda, J.-L., Garcia, N., Gerringa, L., Griffith, B., Guigue, C., Guillerm, C., Jacquet, S., Laan, P., Lefévre, D., Lo Monaco, C., Malits, A., Mosseri, J., Obernosterer, I., Park, Y.-H., Picheral, M., Pondaven, P., Remenyi, T., Sandroni, V., Sarthou, G., Savoye, N., Scouarnec, L., Souhaut, M., Thuiller, D., Timmermans, K., Trull, T., Uitz, J., van Beek, P., Veldhuis, M., Vincent, D., Viollier, E., Vong, L., Wagener, T., 2007. Effect of natural iron fertilization on carbon sequestration in the Southern Ocean. Nature 446, 1070–1074.

Bode, A., Castro, C.G., Dorval, M.D., Varela, M., 2002. New and regenerated production and ammonium regeneration in the western Bransfield Strait region (Antarctica) during phytoplankton bloom conditions in summer. Deep-Sea Res. II 49, 787–804.

Burckle, L.H., Cirilli, J., 1987. Origin of diatom ooze belt in the Southern Ocean: impications for Late Quaternary paleoceanography. Micropaleontol. 33 (1), 82–86.

Burckle, L.H., Jacobs, S.S., McLaughlin, R.B., 1987. Late austral spring diatom distribution between New Zealand and the Ross Ice shelf, Antarctica: hydrographic and sediment correlations. Micropaleontol. 33 (1), 74–81.

Cassar, N., Bender, M.L., Barnett, B.A., Fan, S., Moxim, W.J., Levy II, H., Tilbrook, B., 2007. The Southern Ocean biological response to aeolian iron deposition. Science 317, 1067–1070.

Comiso, J.C., 2003. Large-scale characteristics and variability of global sea ice cover. In: Thomas, D.N., Dieckmann, G.S. (Eds.), Sea Ice: an Introduction to its Physics, Biology, Chemistry, and Geology. Blackwell Science, Oxford, pp. 112–142.

Crosta, X., Pichon, J.-J., Labracherie, M., 1997. Distribution of *Chaetoceros* resting spores in modern peri-Antarctic sediments. Mar. Micropaleontol. 29, 283–299.

Crosta, X., Pichon, J.J., Burckle, L.H., 1998a. Application of modern analog technique to marine Antarctic diatoms: reconstruction of maximum sea ice extent at the Last Glacial Maximum. Paleoceanogr. 13 (3), 284–297.

Crosta, X., Pichon, J.J., Burckle, L.H., 1998b. Reappraisal of Antarctic seasonal sea-ice at the Last Glacial Maximum. Geophys. Res. Letters 25 (14), 2703–2706.

Crosta, X., Sturm, A., Armand, L., Pichon, J.-J., 2004. Late Quaternary sea ice history in the Indian sector of the Southern Ocean as recorded by diatom assemblages. Mar. Micropaleontol. 50, 209–223.

Crosta, X., Romero, O., Armand, L.K., Pichon, J.-J., 2005. The biogeography of major diatom taxa in Southern Ocean sediments: 2. Open ocean related species. Palaeogeogr., Palaeoclimatol. Palaeoecol. 223, 66–92.

Cunningham, W.L., Leventer, A., 1998. Diatom assemblages in surface sediments of the Ross Sea: relationship to present oceanographic conditions. Antarctic Sci. 10 (2), 134–146.

de Baar, H.J.W., de Jong, J.T.M., Nolting, R., Timmermans, K.R., van Leeuwe, M.A., Bathmann, U., Rutgers van der Loeff, M., Sildam, J., 1999. Low dissolved Fe and the absence of diatom blooms in remote Pacific waters of the southern Ocean. Mar. Chemistry 66, 1–34.

de Baar, H.J.W., Boyd, P.W., Coale, K.H., Landry, M.R., Tsuda, A., Assmy, P., Bakker, D.C.E., Bozec, Y., Barber, R.T., Brzezinski, M.A., Buesseler, K.O., Boyé, M., Croot, P.L., Gervais, F., Gorbunov, M.Y., Harrison, P.J., Hiscock, W.T., Laan, P., Lancelot, C., Law, C.S., Levasseur, M., Marchetti, A., Millero, F.J., Nishioka, J., Nojiri, Y., van Oijen, T., Riebesell, U., Rikenberg, M.J.A., Saito, H., Takeda, S., Timmermans, K.R., Veldhuis, M.J.W., Wait, A.M., Wong, C.-S., 2005. Synthesis of iron fertilization experiments: from the Iron Age in the Age of Enlightenment. J. Geophys. Res 110, C09S16. doi:10.1029/2004JC002601.

DeMaster, D.J., 2002. The accumulation and cycling of biogenic silica in the Southern Ocean: revisiting the marine silica budget. Deep-Sea Res. II 49, 3155–3167.

Donahue, J.G., 1973. Distribution of planktonic diatoms in surface sediments of the southern South Pacific. In: Goodell, H.G., et al. (Ed.), Marine Sediments of the Southern Ocean. American Geophysical Society. 18 pp.

Dowdeswell, J.A., Evans, J., Ó Cofaigh, C., Anderson, J.B., 2006. Morphology and sedimentary processes on the continental slope off Pine Island Bay, Amundsen Sea, West Antarctica. GSA Bulletin 118 (5/6), 606–619.

Fenner, J., Schrader, H.-J., Wienigk, H., 1976. Diatom phytoplankton studies in the Southern Pacific Ocean, composition and correlation to the Antarctic convergence and its paleoecological significance. In: Hollister, C.D., et al. (Ed.), Init. Rep. DSDP 35. US Gov. Printing Office, Washington DC, pp. 757–813.

François, R., Altabet, M.A., Yu, E.-F., Sigman, D.M., Bacon, M.P., Frank, M., Bohrmann, G., Bareille, G., Labeyrie, L.D., 1997. Contribution of Southern Ocean surface-water stratification to low atmospheric CO_2 concentrations during the last glacial period. Nature 389, 929–935.

Frenguelli, J., Orlando, H., 1958. Diatomeas y Silicoflagellados del sector Antarctico Sudamericano. Instituto Antarctico Argentino, Publication No 5, Buenos Aires, 191 pp.

Fryxell, G.A., Prasad, A.K.S.K., 1990. *Eucampia antarctica* var. *recta* (Mangin) stat. nov. (Bidduphiaceae, Bacillariophyceae): life stages at the Wedell Sea ice edge. Phycologia 29, 27–38.

Garcia, H.E., Locarnini, R.A., Boyer, T.P., Antonov, J.I., 2006. World Ocean Atlas 2005. In: Levitus, S. (Ed.), Nutrients (Phosphate, Nitrate, Silicate): NOAA Atlas NESDIS 64, U.S. Government Printing Office, Washington, D.C., Vol. 4. 396 pp.

Garibotti, I.A., Vernet, M., Smith, R.C., Ferrario, M.A., 2005. Interannual variability in the distribution of the phytoplankton standing stock across the seas onal sea-ice zone west of the Antarctic Peninsula. J. Plankton Res. 27 (8), 825–843.

Geibert, W., Rutgers van der Loeff, M.M., Usbeck, R., Gersonde, G., Kuhn, G., Seeberg-Elverfeldt, J., 2005. Quantifying the opal belt in the Atlantic and southeast Pacific sector of the Southern Ocean by means of ^{230}Th normalization. Global Biochem. Cycles 19, GB4001. doi:10.1029/2005GB002465.

Gersonde, R., Wefer, G., 1987. Sedimentation of biogenic siliceous particles in Antarctic waters from the Atlantic sector. Mar. Micropaleontol. 11, 311–332.

Gersonde, R., Zielinski, U., 2000. The reconstruction of late Quaternary Antarctic sea ice distribution — the use of diatoms as a proxy for sea ice. Palaeogeogr. Palaeoclimatol. Palaeoecol. 162, 263–286.

Gersonde, R., Abelmann, A., Brathauer, U., Becquey, S., Bianchi, C., Cortese, G., Grobe, H., Kuhn, G., Niebler, H.-S., Segl, M., Sieger, R., Zielinski, U., Fütterer, D.K., 2003a. Last glacial sea surface temperatures and sea-ice extent in the Southern Ocean (Atlantic-Indian sector): a multiproxy approach. Paleoceanogr. 18 (3), 1061. doi:10.1029/2002PA000809.

Gersonde, R., Abelmann, A., Cortese, G., Becquey, S., Bianchi, C., Brathauer, U., Niebler, H.-S., Zielinski, U., Pätzold, J., 2003b. The Late Pleistocene South Atlantic and Southern Ocean surface — a summary of time-slice and time-series studies. In: Wefer, G., Mulitza, S., Ratmeyer, V. (Eds.), The South Atlantic in the Late Quaternary: Reconstruction of Material Budgets and Current Systems. Springer, Berlin, pp. 499–529.

Gersonde, R., Crosta, X., Abelmann, A., Armand, L., 2005. Sea-surface temperature and sea ice distribution of the Southern Ocean at the EPILOG Last Glacial Maximum — a circum-Antarctic view based on siliceous microfossil records. Quat. Sci. Rev. 24, 869–896.

Gouretski, V.V., Koltermann, K.P., 2004. WOCE Global Hydrographic Climatology: A technical report. Berichte des Bundesamtes für Seeschifffahrt und Hydrographie Nr. 35, 52 pp.

Hargraves, P.E., 1968. Species composition and distribution of net plankton diatoms in the Pacific sector of the Antarctic Ocean (Thesis). School of Marine Science, College of Williams and Mary, Virginia. 171 pp.

On the phytoplankton of the south-west Atlantic and the Bellingshausen Sea, 1929–31. Discovery Reports VIII, 1–268.

Hasle, G.R., 1969. An analysis of the phytoplankton of the Pacific Southern Ocean: abundance, composition, and distribution during the *BRATEGG* Expedition, 1947–1948. Hvalradets Skrifter, Scientific Results Of Marine Biological Research, vol. 52. Oslo, 168 pp.

Hasle, G.R., 1976. The biogeography of some marine planktonic diatoms. Deep-Sea Res. 23, 319–338.

Hasle, G., Syvertsen, E.E., 1996. Marine diatoms. In: Tomas, C.R. (Ed.), Identifying Marine Diatoms and Dinoflagellates. Academic Press Limited, London, pp. 5–385.

Hendey, N., 1937. The plankton diatoms of the Southern Seas. Discovery Reports XVI, 151–364.

Hillenbrand, C.-D., 2000. Glaciomarine sedimentation on the continental margins of the Amundsen and Bellingshausen Seas, West Antarctica — indications for paleoenvironmental changes during the Quaternary climatic cycles. Reports on Polar Research, vol. 346. Alfred Wegener Institute for Polar and Marine Research, Bremerhaven. 182 pp.

Holm-Hansen, O., Kahru, M., Hewes, C.D., 2005. Deep chlorophyll *a* maxima (DCMs) in pelagic Antarctic waters. II. Relation to bathymetric features and dissolved iron concentrations. Mar. Ecol. Progr. Ser. 297, 71–81.

Hutchins, D.A., Bruland, K.W., 1998. Iron-limited diatom growth and Si:N uptake ratios in a coastal upwelling regime. Nature 393, 561–564.

Kellogg, D.E., Kellogg, T.B., 1987. Microfossil distributions in modern Amundsen Sea sediments. Mar. Micropaleontol. 12, 203–222.

Kozlova, O.G., 1966. Diatoms of the Indian and Pacific sectors of the Antarctic. National Science Foundation, Israel Program for Scientific Translation, Washington, D.C. 185 pp.

Kunz-Pirrung, M., Gersonde, R., Hodell, D.A., 2002. Mid-Brunhes century scale diatom sea surface temperature and sea ice records from the Atlantic sector of the Southern Ocean (ODP Leg 177, site 1093, 1094 and core PS2089-2). Palaeogeogr. Palaeoclimatol. Palaeoecol. 182, 305–328.

Lutjeharms, J.R.E., Valentine, H.R., 1984. Southern Ocean thermal fronts south of Africa. Deep-Sea Res. A — Oceanogr. Res. Papers 31 (12), 1461–1475.

Mahowald, N.M., Baker, A.R., Bergametti, G., Brooks, N., Duce, R.A., Jickells, T.D., Kubilay, N., Prospero, J.M., Tegen, I., 2005. Atmospheric global dust cycle and iron inputs to the ocean. Global Biogeochem. Cycles 19, GB4025. doi:10.1029/2004GB002402.

Makarenkov, V., Legendre, P., 2002. Nonlinear redundancy analysis and canonical correspondence analysis based on polynomial regression. Ecology 83 (4), 1146–1161.

Miller, H., Grobe, H., 1996. The Expedition ANTARKTIS-XI/3 of RV Polarstern in 1994. Reports on Polar Research, vol. 188. Alfred Wegener Institute for Polar and Marine Research, Bremerhaven. 115 pp.

Monterey, G., Levitus, S., 1997. Seasonal variability of mixed layer depth for the world ocean. NOAA Atlas NESDIS, vol. 14. U.S. Gov. Printing Office, Washington, D.C. 96 pp.

Moore, J.K., Abbott, M.R., 2000. Phytoplankton chlorophyll distribution and primary production in the Southern Ocean. J. Geophys. Res. 105 (C12), 28709–28722.

Nechaev, D.A., Panteleev, G.G., Yaremchuk, M.I., 1997. The circulation in the Amundsen and Bellingshausen seas from atmospheric and oceanic climatic data. Oceanology 37 (5), 586–594.

Nitsche, F.O., Cunningham, A.P., Larter, R.D., Gohl, K., 2000. Geometry and development of glacial continental margin depositional systems in the Bellingshausen Sea. Mar. Geol. 162, 277–302.

Orsi, A.H., Whitworth III, T., Nowlin Jr., W.D., 1995. On the meridional extent and fronts of the Antarctic Circumpolar Current. Deep-Sea Res. I 42 (5), 641–673.

Orsi, A.H., Johnson, G.C., Bullister, J.L., 1999. Circulation, mixing, and production of Antarctic Bottom Water. Progr. Oceanogr. 43, 55–109.

Pichon, J.J., Labracherie, M., Labeyrie, L.D., Duprat, J., 1987. Transfer fuctions between diatom assemblages and surface hydrology in the Southern Ocean. Palaeogeogr. Palaeoclimatol. Palaeoecol. 61, 79–95.

Pichon, J.-J., Bareille, G., Labracherie, M., Labeyrie, L.D., Baudrimont, A., Turon, J.-L., 1992b. Quantification of the biogenic silica dissolution in Southern Ocean sediments. Quat. Res. 37, 361–378.

Pichon, J.-J., Sikes, E.L., Hiramatsu, C., Robertson, L., 1998. Comparison of Uk_{37} and diatom assemblage sea surface temperature estimates with atlas derived data in Holocene sediments from the Southern West Indian Ocean. J. Mar. Systems 17, 541–554.

Pollard, R.T., Read, J.F., Allen, J.T., Griffith, G., Morrison, A.I., 1995. On the physical structure of a front in the Bellingshausen Sea. Deep-Sea Res. II 42 (4–5), 955–982.

Radi, T., Pospelova, V., de Vernal, A., Barrie, J.V., 2007. Dinoflagellate cysts as indicators of water quality and productivity in British Columbia estuarine envirnonments. Mar. Micropaleontol. 62, 269–297.

Ragueneau, O., Tréguer, P., Leynaert, A., Anderson, R.F., Brzezinski, M.A., DeMaster, D.J., Dugdale, R.C., Dymond, J., Fischer, G., François, R., Heinze, C., Maier-Reimer, E., Martin-Jézéquel, V., Nelson, D.M., Quéguiner, B., 2000. A review of the Si cycle in the modern ocean: recent progress and missing gaps in the application of biogenic opal as a paleoproductivity proxy. Global Planet. Change 26, 317–365.

Read, J.F., Pollard, R.T., Morrison, A.I., Symon, C., 1995. On the southerly extent of the Antarctic circumpolar current in the southeast Pacific. Deep-Sea Res. II 42 (4–5), 933–954.

Reid, J.L., 1986. On the total geostrophic circulation of the South Pacific Ocean: flow patterns, tracers and transports. Prog. Oceanogr. 16, 1–61.

Richter, D., Vink, A., Zonneveld, K.A.F., Kuhlmann, H., Willems, H., 2007. Calcareous dinoflagellate cyst distribution in surface sediments from upwelling areas off NW Africa, and relationships with environmental parameters of the upper water column. Mar. Micropaleontol. 63, 201–228.

Robertson Maurice, S.D., Wiens, D.A., Shore, P.J., Vera, E., Dorman, L.M., 2003. Seismicity and tectonics of the South Shetland Islands and Bransfield Strait from a regional broadband seismograph deployment. J. Geophys. Res. 108 (B10), 2461. doi:10.1029/2003JB002416.

Rodehacke, C.B., Hellmer, H.H., Beckmann, A., Roether, W., 2007. Formation and spreading of Antarctic deep and bottom waters inferred from a chlorofluorocarbon (CFC) simulation. J. Geophys. Res. 112, C09001. doi:10.1029/2006JC003884.

Romero, O., Armand, L.K., Crosta, X., Pichon, J.-J., 2005. The biogeography of major diatom taxa in Southern Ocean sediments: 3. Tropical/Subtropical species. Palaeogeogr. Palaeoclimatol. Palaeoecol. 223, 49–65.

Savidge, G., Harbour, D., Gilpin, L.C., Boyd, P.W., 1995. Phytoplankton distributions and production in the Bellingshausen Sea, Austral spring 1993. Deep-Sea Res. II 42 (4–5), 1201–1224.

Sayles, F.L., Martin, W.R., Chase, Z., Anderson, R.F., 2001. Benthic remineralization and burial of biogenic SiO_2, $CaCO_3$, organic carbon, and detrital material in the Southern Ocean along a transect at 170°W. Deep-Sea Res. II 48, 4323–4383.

Scheuer, C., Gohl, K., Udintsev, G., 2006. Bottom-current control on sedimentation in the western Bellingshausen Sea, West Antarctica. Geo-Mar. Lett. 26, 90–101.

Schrader, H.J., Gersonde, R., 1978. Diatoms and silicoflagellates. In: Zachariasse, W.J., et al. (Ed.), Micropaleontological Methods and Techniques — an Exercise on an Eight Metres Section of the Lower Pliocene of Capo Rossello, Sicily: Utrecht Micropaleontol. Bull, vol. 17, pp. 129–176.

Schweitzer, P.N., 1995. Monthly averaged polar sea ice concentration. U.S. Geological Survey Digital Data Series: Virginia. CD rom, Ed 1. DDS-27.

Smetacek, V., Assmy, P., Henjes, J., 2004. The role of grazing in structuring Southern Ocean pelagic ecosystems and biogeochemical cycles. Antarctic Sci. 16 (4), 541–558.

Smith Jr., W.O., Gordon, L.I., 1997. Hyperproductivity of the Ross Sea (Antarctica) polynya during austral spring. Geophys Res. Letters 24 (3), 233–236.

Smith, D.A., Hofmann, E.E., Klinck, J.M., Lascara, C.M., 1999. Hydrography and circulation of the West Antarctic Peninsula Continental Shelf. Deep-Sea Res. I 46, 925–949.

Turner, D.R., Owens, N.J.P., 1995. A biogeochemical study in the Bellingshausen Sea: overview of the STERNA 1992 expedition. Deep-Sea Res. II 42 (4–5), 907–932.

Vink, A., 2004. Calcareous dinoflagellate cysts in South and equatorial Atlantic surface sediments: diversity, distribution, ecology and potential for palaeoenvironmental reconstruction. Mar. Micropalaeontol. 50, 43–88.

von Bodungen, B., 1986. Phytoplankton growth and krill grazing during spring in the Bransfield Strait, Antarctica — implications from sediment trap collections. Polar Biol. 6, 153–160.

Zielinski, U., 1993. Quantitative estimation of palaeoenvironmental parameters of the Antarctic Surface Water in the Late Quaternary using transfer functions with diatoms. Reports on Polar Research, vol. 126. Alfred Wegener Institute for Polar and Marine Research, Bremerhaven. 148 pp.

Zielinski, U., Gersonde, R., 1997. Diatom distribution in Southern Ocean surface sediments (Atlantic sector): implications for paleoenvironmental reconstructions. Palaeogeogr., Palaeoclimatol., Palaeoecol. 13 (129), 213–250.

Zielinski, U., Gersonde, R., Sieger, R., Fütterer, D., 1998. Quaternary surface water temperature estimations: calibration of a diatom transfer function for the Southern Ocean. Paleoceanogr. 13 (4), 365–383.